Mechanical Systems and Signal Processing 245 (2026) 113836

Contents lists available at ScienceDirect

Mechanical Systems and Signal Processing

journal homepage: www.elsevier.com/locate/ymssp

Full length article

Model updating and model selection for structural structures via Approximate Bayesian Computation

A. Ben Abdessalem [a,*], N. Dervilis [b], D. Wagg [b], K. Worden [b]

[a] Univ Angers, LARIS, SFR, MATHSTIC, F-49000, France
[b] Dynamics Research Group, School of Mechanical, Aerospace and Civil Engineering, University of Sheffield, Mappin Street, Sheffield S1 3JD, United Kingdom

ARTICLE INFO

Communicated by I. Kougioumtzoglou

Keywords:
Approximate Bayesian methods
Model updating & model selection
Uncertainty quantification
Simulation-based method
MVEE
Modal data

ABSTRACT

Approximate Bayesian methods, or "likelihood-free" methods, have become a key component of modern statistical methodology, providing a framework for inference, prediction, and decision-making. Their versatility lies in their ability to handle parameter estimation, model selection, and uncertainty quantification within a unified probabilistic framework. In this work, Approximate Bayesian Computation (ABC) using an ellipsoidal Nested Sampling (NS) approach is employed to deal with model updating and model comparison issues applied to structural health monitoring. ABC methods rely essentially on the ability to simulate data from a simulator/forward model, bypassing the need to write down an explicit likelihood function, which is always far from trivial. These methods are particularly captivating because of the modelling freedom they provide; in addition, they are flexible in the sense that different discrepancy functions measuring the similarity between the observed modal data and the corresponding model output can be used. However, Bayesian inference methods usually require numerous forward model simulations to generate converged samples. To enhance the computational efficiency of the sampler, the *minimum-volume enclosing ellipsoid* (MVEE) is incorporated to better enclose the accepted particles and to guide the sampler more efficiently towards the highest probability region. The performance and the robustness of the novel sampler in structural model updating and model selection is demonstrated here via different numerical studies using modal data.

1. Introduction

Model updating refers to an iterative process where the primary goal is to find the most probable parameters in a computational model by minimising the discrepancies between the model predictions and the measured data from the physical structure [1]. The updated model gives engineering practitioners a variety of benefits in model-based tasks, such as damage detection, risk and reliability assessment, structural control, and failure prognostics [2,3]. The quality of the model updating depends on the class of mathematical model chosen, and the measurement errors. Consequently, a unified probabilistic framework handling parameter calibration and model selection becomes a useful option for practitioners. While many studies have dealt with the subject of model updating, relatively little attention has been given to model selection applied in the context of structural health monitoring (SHM). Often several plausible models, each describing a different hypothesis could fit the data. These models can then be fitted

* Corresponding author.
E-mail address: anis.ben-abdessalem@univ-angers.fr (A. Ben Abdessalem).

https://doi.org/10.1016/j.ymssp.2025.113836
Received 4 August 2025; Received in revised form 23 November 2025; Accepted 29 December 2025

to experimental data and systematically compared to each other, and this is the second topic touched in this paper in addition to model updating for a single model.

As already mentioned, different approaches have been proposed in the literature to consider the problem of model updating, which can be classified into two main categories. *Deterministic approaches* which provide single point estimate of the expected values of parameter such that the discrepancies between model output and dynamic measurement data are minimised have been successfully applied. An overview of deterministic updating techniques can be found in [4]. In the last two decades, the focus has shifted to *Bayesian methods* for model updating. Bayesian methods provide a robust and coherent framework for updating and uncertainty quantification of models by making use of measured response, following probability rules in the treatment of uncertainty. For this reason, increasing attention has been given to probabilistic methods, among which the most common is Markov Chain Monte Carlo (MCMC) sampling [5]. A general discussion of MCMC sampling in the scope of Bayesian updating of structural models is given in [6]. Examples of MCMC methods and other variants thereof applied to Bayesian updating in structural dynamics include Gibbs-sampling [7] or evolutionary MCMC methods [8–10]. Another useful alternative for Bayesian model updating is Transitional Markov chain Monte Carlo (TMCMC) proposed by Ching and Chen [11]. TMCMC aims to sample from intermediate probability density functions (PDFs) that gradually converge to the target PDF, rather than directly sampling from the target PDFs, which can be challenging. Betz et al. [12] discussed the properties of TMCMC and proposed modifications to improve efficiency (see, e.g., [13,14] for other recent developments). An alternative approach to MCMC is the Bayesian Updating with Structural reliability methods (BUS) approach, which employs sampling-based structural reliability methods to sample from the posterior distribution [15]. Application of the BUS approach combined with subset simulation to structural identification problems can be found in [15–17]. In Ref. [18], a two-stage Bayesian model updating framework based on an affine-invariance sampling in TMCMC algorithm is proposed. Yang et al. [19] developed an enhanced adaptive sequential Monte Carlo method (EASMC) to solve both Bayesian model updating and model class selection in a unified manner. Monchetti et al. [20] investigated strengths and weaknesses of two different Bayesian methods: Bayesian Model Updating (BMU) and Approximate Bayesian Computation (ABC) for model identification of masonry towers using dynamic data. The authors conclude that the two procedures have achieved very similar results, even though there is no clear winner in the comparison. Ereiz et al. [21] give a review of the most-used approaches in finite-element model updating (FEMU) of civil-engineering structures, focusing on the iterative stochastic and deterministic methods and the process of their application. Seung-Seop et al. [22] proposed a new FEMU method based on mixed-integer nonlinear programming (MINLP) which can explore both model and parameter space simultaneously. The performance of the proposed method has been demonstrated on numerical and experimental case studies and has been compared with conventional FEMU methods. Zeng and Kim [23] presented a novel Bayesian model updating approach for damage detection, where a new likelihood function was introduced to address the coupling effect between mass and stiffness parameters. Henikish et al. [24] proposed Bayesian model-updating to detect damage for a lab-scale three-storey shear building using complex modal data and dynamic model reduction. Yuan et al. [25] proposed an active-learning structural damage detection framework based on a Kriging surrogate model and Bayesian inference for a multisensory vehicle-bridge system. In Ref. [26], the author proposed a practical framework for structural FEMU and damage prediction based on the Bayesian regularisation with incomplete modal data. Kiran et al. [27] proposed a Bayesian model updating method for updating structural FE models and damage detection using strain-based modal data. Here, dynamic model reduction is incorporated into the proposed framework in order to reduce the dimensionality of the problem. An iterative Metropolis–Hasting (MH)–within-Gibbs sampler is proposed to simulate the samples following the posterior PDF. Waeytens et al. [28] presented a comparative study of deterministic and probabilistic model updating, considering different types of regularisation technique; such techniques include classical Tikhonov regularisation, constitutive relation error-based regularisation, and Bayesian regularisation, all of which were applied to damage detection.

Despite the widespread success of Bayesian inference in model updating in the context of SHM, several challenges remain. One key limitation is the reliance on an explicit likelihood function, which is often difficult to evaluate or in some circumstances to formulate, especially in complex models and data structures where the likelihood is intractable. In addition, the likelihood-based approaches usually utilises MCMC to estimate posterior distributions, which requires a significant number of model runs to ensure convergence. This makes MCMC computationally expensive, particularly for large-scale engineering structures. In recent years, likelihood-free inference (LFI) such as approximate Bayesian computation has emerged as a viable alternative for cases where the likelihood function is either unavailable or intractable; it is one of the most developed forms of likelihood-free inference. The ABC algorithms bypass the need for explicit likelihood functions by using a simulator to generate synthetic data. In ABC, one compares simulated data with real observations using an “accept–reject” mechanism based on predefined thresholds [29]. LFI methods rely essentially on the ability to simulate data from a simulator/forward model bypassing the need to write down a likelihood function which is always far from trivial. Simulator-based models are particularly captivating because of the modelling freedom that they provide. In essence, any data-generating mechanism that can be written as a finite set of algorithmic steps can be programmed as a simulator-based model. Moreover, different metrics from the time-domain or frequency-domain can be used to formulate the discrepancy function. Since its inception, different variants have been proposed in the literature to improve the ABC efficiency. Chiachio et al. [30] developed a new algorithm, called ABC-SubSim, by incorporating the Subset Simulation algorithm [31] for rare-event simulation into the ABC algorithm. Later, Vakilzadeh et al. [32] applied the ABC-SubSim to infer unknown model parameters and select models on nonlinear dynamic systems. Yang and Lam [33] applied an adaptive sequential Monte Carlo method for model updating and damage detection in two experimental rigs. Zeng et al. [34] investigated a likelihood-free Bayesian inference method named BayesFlow that approximates the posterior distributions by jointly training a conditional invertible neutral network (cINN) for probabilistic damage inference. Ni et al. [35] proposed a likelihood-free Bayesian inference approach for structural condition assessment with output-only vibration responses for which an adaptive Gaussian surrogate model is proposed to approximate the

likelihood function. Fakih et al. [36] combined the ABC-SubSim method with ANN-based surrogate models for damage identification in welded structures. Ben Abdessalem et al. [37] used the ABC-SMC method proposed by Toni et al. [38] to select the most suitable model on a structural dynamics problem. Ritto et al. [39] combined the standard ABC algorithm with a reinforcement learning technique to accelerate the sampler. The effectiveness of their method has been demonstrated through updating parameter estimation and model predictions to time-varying systems. In this work, a simulation-based inference procedure based on Approximate Bayesian Computation coupled with an ellipsoidal nested-sampling technique is employed to deal with model updating and model-selection issues applied to structural health monitoring. The main novelty lies in the use of the concept of *minimum-volume enclosing ellipsoid* to better enclose the drawn particles which map prior samples to posterior samples. In the paper, we go through various numerical experiments to deal with model updating and model selection in the context of SHM, illustrating the versatile features of ABC in practice.

The remainder of this paper is outlined as follows: Section 2 formulates the problem of structural model updating. Section 3 details the basic concepts of the ABC framework, and gives the implementation procedures with a focus on the main novelties to enhance the computational efficiency. In Section 4, the computational efficiency of the improved ABC-NS sampler is demonstrated via two engineering structures. Finally, a conclusion of the work is presented, with some future directions in Section 5.

2. Structural model updating formulation

2.1. Frequency-domain formulation

Frequency-domain approaches update a finite element (FE) model using measured modal properties such as natural frequencies, damping ratios and vibration mode shapes. These modal properties can be obtained from vibration tests and compose the measured data. A set of modal data is expressed as:

$$\mathcal{D} = \left\{ \omega_1^m, (\varphi_1^m)^{\mathrm{T}}, \omega_2^m, (\varphi_2^m)^{\mathrm{T}}, \dots, \omega_{n_m}^m, (\varphi_{n_m}^m)^{\mathrm{T}} \right\}^{\mathrm{T}}, \quad i = 1, \dots, n_m \tag{1}$$

where ω_i^m is the ith natural frequency, φ_i^m is the ith mode shape vector (superscript "m" refers to measured), and n_m is the number of modes.

It should be noted that experimentally identified mode shapes $\{\varphi_i^m\}$ are only available at measured degrees of freedom (DOFs). On the other hand, modal properties of the structure can be calculated by solving the generalised eigenvalue problem in structural dynamics:

$$\left(\mathbf{K}(\theta) - \omega_i^2 \mathbf{M}\right)\varphi_i = 0, \quad i = 1, 2, \dots, n_m \tag{2}$$

where $\mathbf{M}$ and $\mathbf{K}$ are the mass and stiffness matrices, respectively; ω_i and φ_i are the ith natural frequency and mode shape of the structure, respectively. It is important to note that only stiffness coefficients (denoted by the vector θ) are considered model parameters, and the mass is kept constant.

The FE model has a stiffness matrix $\mathbf{K}$, parametrised here as follows:

$$\mathbf{K}(\theta) = \sum_{i=1}^{n_e} \theta_i \mathbf{k}_i \tag{3}$$

where $\mathbf{k}_i$ is the ith element stiffness matrix, θ_i is the ith element stiffness coefficient to be updated according to the observed data $\mathcal{D}$, and n_e is the number of structural elements.

For a set of parameters θ, the parameter-to-modal properties map giving the simulated modal properties $\mathcal{D}_s$, is made via a simulator/forward model; it is given as:

$$\mathcal{D}_s := \mathcal{M}(\theta) = \left\{ \omega_1^s, (\varphi_1^s)^{\mathrm{T}}, \omega_2^s, (\varphi_2^s)^{\mathrm{T}}, \dots, \omega_{n_m}^s, (\varphi_{n_m}^s)^{\mathrm{T}} \right\}^{\mathrm{T}}, \quad i = 1, \dots, n_m \tag{4}$$

The superscript/superscript "s" refer to simulated. The parameters of the model can be inferred by minimising the discrepancy between simulated and experimental modal properties.

2.2. Definition of a discrepancy function

Besides the choice of the updated parameters, the formulation of the discrepancy function is another important ingredient in the process of model updating. The discrepancy function compares the measured data with the data obtained from the simulator; for this reason, it has to be sensitive to small changes in the structural behaviour. In this paper, model updating is based on the natural frequencies and mode shapes, since these dynamic features can be obtained experimentally in relatively high quality. The discrepancy function aims at achieving a close match between measured and predicted modal parameters and is given here by Eq. (5) although other choices are also possible:

$$\rho(\mathcal{D}, \mathcal{D}_s) = \sum_{i=1}^{n_m} \left(\frac{\omega_i^m - \omega_i^s(\theta)}{\omega_i^m} \right)^2 + \sum_{i=1}^{n_m} \left(1 - \mathrm{MAC}_i(\theta)\right) \tag{5}$$

The first term measures the discrepancy between the measured and simulated frequencies. The second term determines the degree of similarity between two mode-shape vectors in terms of the modal assurance criterion (MAC). The MAC value bounds a value of 0 to 1, is a widely-used metric to compare two mode shape vectors and is defined as:

$$\mathrm{MAC}_i = \frac{\left|\varphi_i^{m\mathrm{T}}\varphi_i^s\right|^2}{(\varphi_i^{m\mathrm{T}}\varphi_i^m)(\varphi_i^{s\mathrm{T}}\varphi_i^s)} \tag{6}$$

where φ_i^m is the ith measured mode shape and $\varphi_i^s = \varphi_i^s(\theta)$ is the ith simulated mode shape.

2.3. Modelling of noise

Measurement data from experimental modal testing in the laboratory or field are usually prone to systematic errors because of the inaccuracy of measurement devices, data processing errors or because of human factors. So, the natural frequencies and mode shapes obtained numerically from the finite-element (FE) model here are polluted with noise to generate realistic measurements. In this study, noise is added to the frequencies and modes shapes using Eqs. (7) and (8), respectively.

$$\omega_i^{noise} = \Big(1 + e_\omega(2\mathrm{rand} - 1)\Big)\omega_i \tag{7}$$

$$\varphi_i^{noise} = \big(1 + e_\varphi(2\mathrm{rand} - 1)\big)\,\varphi_i \tag{8}$$

where ω_i^{noise} is the ith natural frequency contaminated by noise and φ_i^{noise} is the ith mode shape vector polluted by noise; (e_ω, e_φ) represent the degree of noise being added and "rand" represents a uniformly distributed vector of random numbers between $[0, 1]$.

It is widely recognised that the natural frequencies are least contaminated by measurement noise and can generally be measured with higher accuracy in comparison with mode shapes.

3. Bayesian-inference methods

3.1. Bayes formalism

Bayesian inference has proven very efficient to deal with parameter estimation and model selection in many disciplines. It consists of assessing the relative plausibility of a set of candidate models $\mathbf{M} = \{\mathcal{M}_k, k = 1, \ldots, \kappa\}$ as well as the parameters θ within each model (for simpler presentation, a subscript k on θ is omitted) using a combination of one's prior knowledge and a set of measured data, $\mathcal{D}$. Both levels of inference (i.e., parameter estimation and model selection) can be addressed via the sequential application of Bayes' theorem:

$$\mathbb{P}(\theta|\mathcal{D}, \mathcal{M}_k) = \frac{\mathbb{P}(\mathcal{D}|\theta, \mathcal{M}_k)\mathbb{P}(\theta|\mathcal{M}_k)}{\mathbb{P}(\mathcal{D}|\mathcal{M}_k)} \tag{9}$$

$$\mathbb{P}(\mathcal{M}_k|\mathcal{D}) = \frac{\mathbb{P}(\mathcal{D}|\mathcal{M}_k)\mathbb{P}(\mathcal{M}_k)}{\mathbb{P}(\mathcal{D})} \tag{10}$$

Evaluation of Eq. (9) requires the definition of the prior, $\mathbb{P}(\theta|\mathcal{M}_k)$, and the likelihood, $\mathbb{P}(\mathcal{D}|\theta, \mathcal{M}_k)$. The prior is a subjective probability distribution which describes one's prior belief for the parameter values. The likelihood encodes the information contained in the data according to model $\mathcal{M}_k$, with parameters θ. The denominator of Eq. (9) is a normalising constant which ensures that $\mathbb{P}(\theta|\mathcal{D}, \mathcal{M}_k)$ integrates to unity. Successful evaluation of Eq. (9) gives the posterior parameter distribution, which describes the probability of parameter vector θ, given the data $\mathcal{D}$, and the chosen model structure $\mathcal{M}_k$.

With regard to Eq. (10), $\mathbb{P}(\mathcal{M}_k)$ is the prior probability of $\mathcal{M}_k$, that expresses the modeller's judgement on the initial relative plausibility of $\mathcal{M}_k \in \mathbf{M}$, before observing data $\mathcal{D}$. Prior model probability $\mathbb{P}(\mathcal{M}_k)$ can be specified depending on the existing prior knowledge about the credibility of model $\mathcal{M}_k$, or it can be given a uniform probability, $\mathbb{P}(\mathcal{M}_k) = 1/\kappa$, if not referring to any information. $\mathbb{P}(\mathcal{D})$ is a normalising constant and $\mathbb{P}(\mathcal{D}|\mathcal{M}_k)$ is equal to the evidence term on the denominator of Eq. (9). $\mathbb{P}(\mathcal{M}_k|\mathcal{D})$ is a distribution describing the relative probability of different competing model structures conditional on the data, $\mathcal{D}$.

3.2. Likelihood-free method

To deploy ABC methods, one needs to be able to simulate data from the model, and requires a distance function, $\rho(\mathcal{D}, \mathcal{D}_s)$, where $\mathcal{D}_s$ is the simulated data generated via the simulator/forward model. This distance function provides a measure of discrepancy between the observed and the simulated data. After calculating $\rho(\mathcal{D}, \mathcal{D}_s)$, one accepts the particle θ when $\rho(\mathcal{D}, \mathcal{D}_s) \leq \varepsilon$, where ε is the tolerance threshold. This condition leads to a modification of the original Bayes theorem (see, Eq. (9), the model is dropped for simplicity):

$$\mathbb{P}(\theta|\rho(\mathcal{D}, \mathcal{D}_s) \leq \varepsilon) = \frac{\mathbb{P}(\rho(\mathcal{D}, \mathcal{D}_s) \leq \varepsilon|\theta)\mathbb{P}(\theta)}{\mathbb{P}(\rho(\mathcal{D}, \mathcal{D}_s) \leq \varepsilon)} \tag{11}$$

For the prior probability distribution, $\mathbb{P}(\theta)$, a uniform prior will be assumed over the possible parameter set θ. By being able to produce simulations from the simulator, inference for the parameters of interest subject to data $\mathcal{D}$ becomes possible. The tolerance threshold ε determines the level of approximation; as $\varepsilon \to 0$, $\mathbb{P}(\theta|\rho(\mathcal{D}, \mathcal{D}_s) \leq \varepsilon) \to \mathbb{P}(\theta|\mathcal{D})$.

Conversely to classical Bayesian inference, the ABC algorithm brings a straightforward solution to approximate $\mathbb{P}(\mathcal{M}_k|\mathcal{D})$ (see [40,41]). Briefly, a model $\mathcal{M}_k$ is sampled from the prior and the model is stored only if the difference between simulated data and the observed data is less than a prefixed threshold. The posterior probability $\mathbb{P}(\mathcal{M}_k|\mathcal{D})$ is then approximated by the acceptance frequency of $\mathcal{M}_k$. When no prior information is available for the preference of the models, one assumes that the prior on the models follows a uniform distribution. As a result, comparing $\mathbb{P}(\mathcal{M}_k|\mathcal{D})$ is the same as comparing $\mathbb{P}(\mathcal{D}|\mathcal{M}_k)$, and the model with the largest value of $\mathbb{P}(\mathcal{D}|\mathcal{M}_k)$ should be selected. In the literature, $\mathbb{P}(\mathcal{D}|\mathcal{M}_k)$ is known as the Bayesian evidence or the marginal likelihood under model $\mathcal{M}_k$, and it has also been widely used for model selection (e.g., see [42,43]). The most elementary implementation of ABC is ABC rejection sampling (ABC-RS) [44,45], (see, Algorithm 1 for parameter estimation and Algorithm 2 for model comparison).

Algorithm 1 ABC-RS FOR PARAMETER ESTIMATION

Input: Given a set of observations $\mathcal{D}$, a simulator (model) $\mathcal{M}(\bullet)$, a tolerance level ε, and a discrepancy metric $\rho(\bullet)$:
for $i = 1, \dots, \mathrm{N}$ **do**
  repeat
    Generate θ^* from the prior $\mathrm{P}(\cdot)$
    Generate $\mathcal{D}_s$ from the simulator/forward FE model $\mathcal{M}(\cdot|\theta^*)$
    Compute $\rho_i = \rho(\mathcal{D}, \mathcal{D}_s)$
  until $\rho(\mathcal{D}, \mathcal{D}_s) \leq \varepsilon$,
  Set $\theta_i = \theta^*$
Output: A set of values $(\theta_1, \dots, \theta_{\mathrm{N}})$ from $\mathrm{P}_\varepsilon(\theta|\mathcal{D}, \mathcal{M})$

Algorithm 2 ABC-RS FOR MODEL SELECTION

Input: Given a set of observations $\mathcal{D}$, a set of possible models $\{\mathcal{M}_1, \mathcal{M}_2, \dots, \mathcal{M}_\kappa\}$, a tolerance level ε, and a discrepancy metric $\rho(\bullet)$:
for $i = 1, \dots, \mathrm{N}$ **do**
  repeat
    Generate $\mathcal{M}^*$ from $\mathrm{P}(\mathcal{M}_k)$, $k = 1, \dots, \kappa$
    Generate θ^* from $\mathrm{P}_k(\theta_k)$
    Generate $\mathcal{D}_s$ from the simulator/forward FE model $\mathcal{M}(\cdot|\theta^*)$
  until $\rho(\mathcal{D}, \mathcal{D}_s) \leq \varepsilon$
  Set $\mathcal{M}^{(i)} = \mathcal{M}^*$ and $\theta^{(i)} = \theta^*_{k^*}$
Output: A set of values $(\mathcal{M}^{(1)}, \dots, \mathcal{M}^{(\mathrm{N})})$ and $(\theta^{(1)}, \dots, \theta^{(\mathrm{N})})$ from $\mathrm{P}_\varepsilon(\mathcal{M}_k|\mathcal{D})$ and $\mathrm{P}_{\varepsilon,k}(\theta_k|\mathcal{D}, \mathcal{M}_k)$, for $k = 1, \dots, \kappa$, respectively.

These algorithms are computationally inefficient, because they sample blindly over the model and parameter space and also because always the highest posterior region defines a relatively small region of the parameter space which needs a significant number of model runs. In recent years, several new variants have been developed in the literature to overcome this issue. In the present study, the ABC algorithm coupled with an elegant nested sampling technique (ABC-NS) introduced in previous work [46] is employed. The next section details the algorithmic implementation of the inference scheme with a focus on the main novelty.

3.3. Algorithmic implementation of the improved ABC-NS sampler

The ABC-NS algorithm is an advanced sampler to deal with parameter estimation and model selection in a unified probabilistic framework. The algorithm explores the posterior distribution by producing a series of nested ellipsoids based on the accepted particles which map prior samples to posterior samples by progressively decreasing a tolerance threshold. The pseudo-code given in Algorithm 3 provides an overview of the iterative process in the ABC-NS sampler. The algorithm starts by selecting a model from the candidate models supposed to be equally probable. A proposal particle is then sampled from the prior over the model parameters, simulating the data using the simulator and keep the pair (model, particle) if the constraint $\rho(\bullet) \leq \varepsilon_1$ is satisfied. The simulations are repeated until one gets N particles distributed over the candidate models. Weights are then calculated for each particle and normalised according to each model using the kernel shown in line 13 [47]. The weighting function plays a crucial role in the inference process. It promotes good solutions and it helps the algorithm to converge towards the highest probability density region. The first iteration of the ABC-NS algorithm is similar to the vanilla ABC-RS algorithm 2 but with a large tolerance threshold value to speed-up the algorithm in the first round.

The subsequent tolerance threshold is defined based on the discrepancy values ranked in descending order (highest on top, see, line 14) as the $(\alpha_0\mathrm{N})$-th value where α_0 is an hyper-parameter defined by the user and which corresponds to the proportion of rejected particles. After that, one normalises the weights of the remaining particles (see, line 17) and a weight of zero is assigned to the rejected particles. From the remaining particles, a proportion equal to $(\beta_0\mathrm{N})$ are randomly selected and propagated to the next population (β_0 is a second hyperparameter). The "alive" particles associated to each model are then enclosed in an ellipsoid

in which the centre point and the covariance matrix are computed as follows:

$$\mu^{(1)} = \frac{1}{\mathrm{N}_\beta} \sum_{i=1}^{\mathrm{N}_\beta} \theta_1^{(i)} \tag{12}$$

$$\mathbf{A}^{(1)} = \frac{1}{\mathrm{N}_\beta - 1} \sum_{i=1}^{\mathrm{N}_\beta} \left(\theta_i^{(1)} - \mu^{(1)}\right)\left(\theta_i^{(1)} - \mu^{(1)}\right)^{\mathrm{T}} \tag{13}$$

where N_β is the number of alive particles and $\{\theta_i^{(1)}\}_{i=1}^{\mathrm{N}_\beta}$ denotes the vector of those particles. One denotes this ellipsoid by $\mathcal{E}^{(1)} = (\mu^{(1)}, \mathbf{A}^{(1)})$. Here, this enclosing ellipsoidal method is referred to the COV-approach.

The main novelty here in the improved ABC-NS sampler is to introduce the *minimum-volume enclosed ellipsoid* (MVEE) technique to enclose the remaining particles which better delimits the parameter space. Basically, the MVEE is an important tool in robust outlier detection in statistics. There are other methods that can be used for this purpose such as the Minimum Covariance Determinant Estimator of [48] or distance-based methods as in [49]. Consider a set of N_β particles in an n-dimensional space: $S = \{\theta_1, \ldots, \theta_n\} \in \mathbb{R}^n$. Denote the MVEE of the set S by MVEE(S). The ellipsoid should have a positive volume and in centre form is given by Moshtagh [50]:

$$\mathcal{E}(\mu, \mathbf{A}) := \left\{ \theta \in \mathbb{R}^d \,:\, (\theta - \mu)^{\mathrm{T}} \mathbf{A} (\theta - \mu) \leq 1 \right\} \tag{14}$$

where $\mathbf{A}$ is a symmetric positive definite matrix ($\mathbf{A} \succ 0$) of order $n \times n$ and μ represents its centre point (superscript/subscript are dropped for simplicity).

The MVEE problem is then to find μ and $\mathbf{A}$ that minimise the volume of $\mathcal{E}$ subject to the constraint that all points θ_i are contained within $\mathcal{E}$. The volume of $\mathcal{E}$ is given by the following formula:

$$\mathrm{Vol}\left(\mathcal{E}(\mu, \mathbf{A})\right) = \frac{\pi^{n/2}}{\Gamma(\frac{n}{2} + 1)\sqrt{\det(\mathbf{A})}} \tag{15}$$

where $\det(\cdot)$ denotes the matrix determinant, $\Gamma(\cdot)$ is the Gamma function, and n is the dimension of the parameter space.

By definition, the MVEE is defined as the smallest ellipsoid (of minimum volume) that contains all the particles. Formally, from Eqs. (14) and (15) the problem of finding the MVEE can be formulated as:

$$\begin{cases} \underset{\mathbf{A}>0,\ \mu}{\text{Minimise}} & \det\left(\mathbf{A}\right) \\ \text{subject to} & \left(\theta_i - \mu\right)^{\mathrm{T}} \mathbf{A} \left(\theta_i - \mu\right) \leq 1, \forall i = 1, \ldots, m \end{cases} \tag{16}$$

This formulation features a simplified convex-optimisation problem [50]; therefore, the global optima can be determined by a mathematical programming method. There are several different methods available in order to obtain a solution of the problem; the one used here is the dual formulation method based on Khachiyan's algorithm [50–55]. The Khachiyan algorithm finds the minimum volume ellipsoid by an iterative procedure constructing a sequence of decreasing ellipsoids. For more details of the applied algorithm and method, readers can look to the previous references where there is a complete analytical description.

In order to illustrate how the algorithm works, a synthetic data matrix of dimensions 3×200 was constructed with each column a randomly generated vector from a normal distribution with zero mean and unit standard deviation. A tolerance parameter can be used to allow a proportion of points to escape the ellipse which was set to 0.1 and the MVEE was calculated. Fig. 1(a) shows the synthetic data, while in Figs. 1(b) and 1(c), one can see how each approach encapsulates the data points. Clearly the MVEE-approach leads to a tighter boundary compared with the COV-approach. A computation of the ellipsoid volume gives a value of 153.62 for the COV-approach against 116.25 with the MVEE-approach. A reduction in volume of almost 25%. Fig. 2 projects onto the data a 2D plane to show the way that the points are enclosed using both approaches. The beauty of this approach is that it extends naturally to high-dimensional data. Thus it is embedded in the ABC-NS sampler to better delimit the most important region in the parameter space.

The subsequent tolerance threshold is defined based on the discrepancy values ranked in descending order (highest on top, see, line 14) as the $(\alpha_0 \mathrm{N})$-th value where α_0 is equal to 0.3. After that, one normalises the weights of the remaining particles (see, line 17) and a weight of zero is assigned to the rejected particles. From the remaining particles, a number of $(\beta_0 \mathrm{N})$ are probabilistically selected and propagated to the next population. The "alive" particles associated to each model are then enclosed in an ellipsoid. Finally, the population is replenished by re-sampling particles inside the defined ellipsoid for each model (see lines 21–29) following the scheme in [56] which consists to sample inside nested ellipsoids. In the subsequent steps, the threshold is updated adaptively in the same way and sample selections are subjected to more stringent threshold. The priors on the models are also continuously updated over the iterations. Through the populations and as $\varepsilon \to 0$, a larger number of particles are selected for the most likely model(s) and the samples for the parameters better reflect the real posterior distribution. Several stopping criterions could be used to stop the algorithm. In this work, the algorithm is stopped when the difference between two successive tolerance threshold values falls below a pre-specified value.

At the last population, the algorithm produces a Markov chain on $(\mathcal{M}, \theta)$ for which the marginal distribution is $\mathbb{P}(\mathcal{M}|D)$. Suppose one has obtained $(\mathcal{M}_k^{(i)}, \theta_k^{(i)})$ with $(i = 1, \ldots, \mathrm{N}, k = 1, \ldots, \kappa)$ at the last population; the posterior model probability can then be estimated by:

$$\widehat{\mathbb{P}}(\mathcal{M}_k|D) = \frac{1}{\mathrm{N}} \sum_{i=1}^{\mathrm{N}} \mathbb{I}(\mathcal{M}^{(i)} = \mathcal{M}_k), \quad k = 1, \ldots, \kappa \tag{17}$$

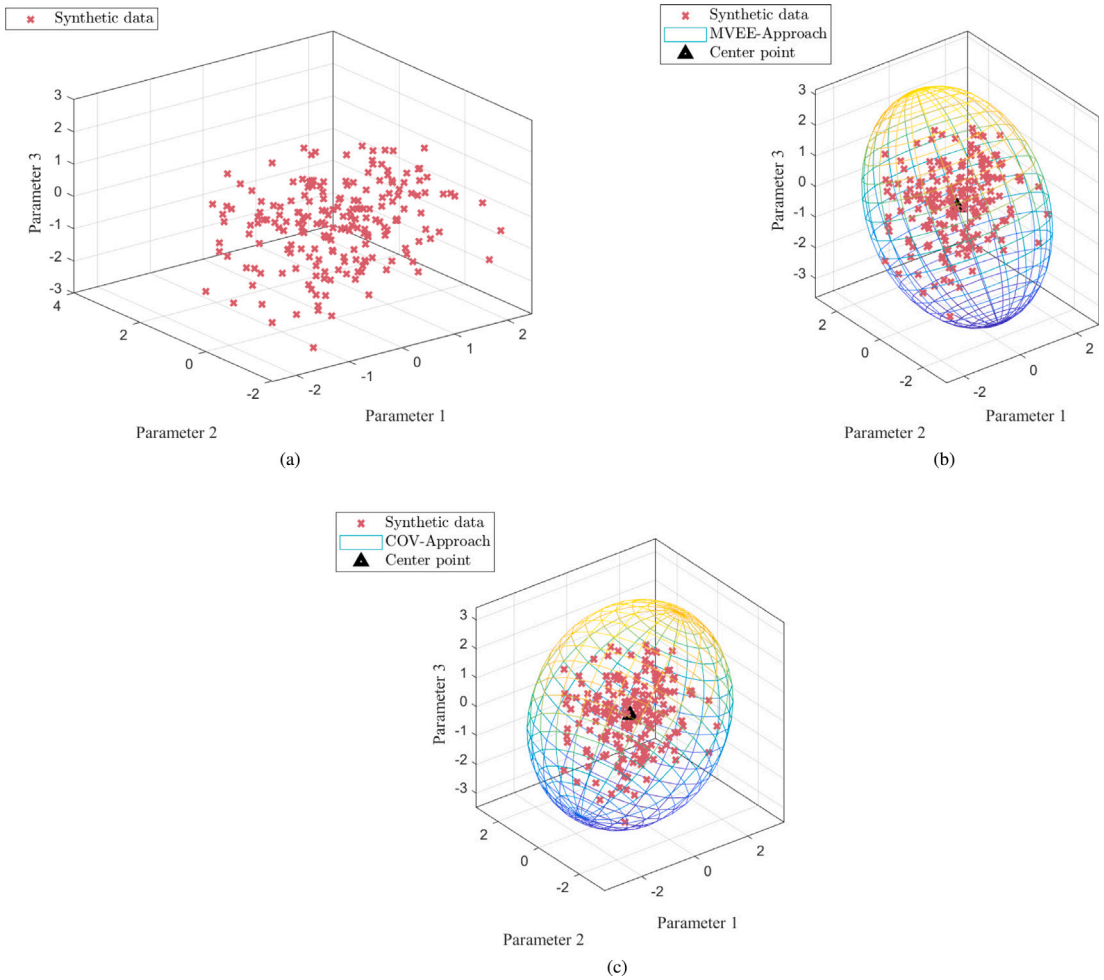

Fig. 1. Illustrations of the ellipsoidal fitting using COV and MVEE approaches.

where $\mathbb{I}(\cdot)$ denotes the indicator function.

Additionally, a shrinking factor is defined in order to eliminate much earlier non-promising particles on the boundary based on the fact that the samples lying on or close to the boundary can be viewed as the samples with the highest distances. This factor is decreasing over the iterations t, and defined by the following equation:

$$G(t) = G_0 \exp\left(1 - \frac{t}{t_{\max}}\right) \tag{18}$$

where G_0 is a constant and $t_{\max}$ is the maximum number of iterations. In this paper, it is assumed that the total number of iterations is fixed at 500. Consequently, G_0 is calibrated to get $G(t = 1) = 1$. Algorithm 3 is run for $t_{\max}$ iterations used as an additional stopping criterion.

Hyperparameter setup: all the numerical examples, consider N = 1000 particles, $\alpha = 0.3$ (30% of the particles are dropped), $\beta = 0.6$ (60% is the percentage of the alive particles), $t_{\max} = 500$. Stopping criterion as being reached when the difference between two successive tolerance thresholds is less than a predefined error ξ_{tol}.

4. Numerical case studies

In this section, the improved ABC-NS sampler is verified via three different case studies with and without noise. The obtained results are compared with the ones from original sampler. All numerical-simulation investigations are performed in the MATLAB® environment on an Intel Core (TM) i7-12800H, 2.40 GHz CPU processor, 32 GB RAM.

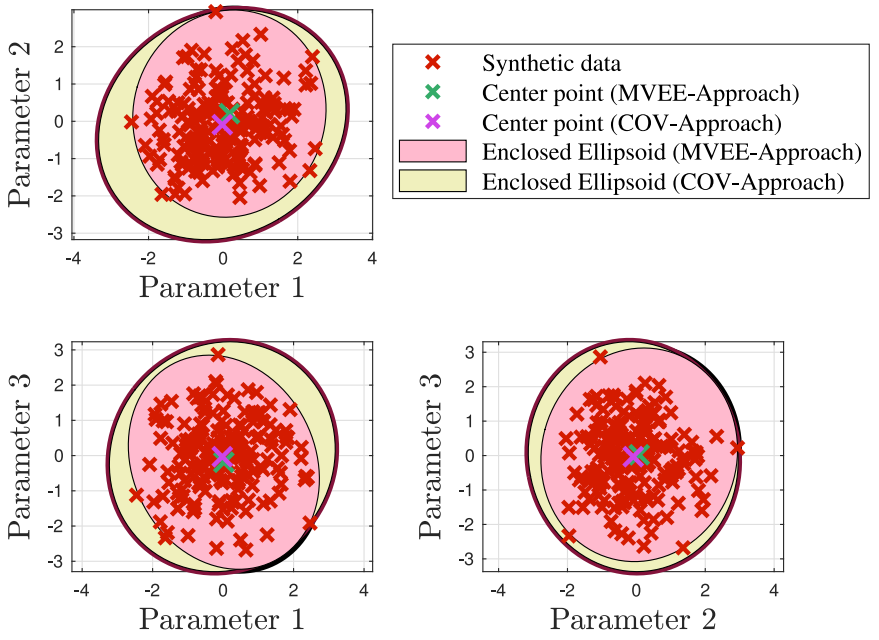

Fig. 2. Illustrations of the ellipsoidal fitting using the same data projected on 2D plane.

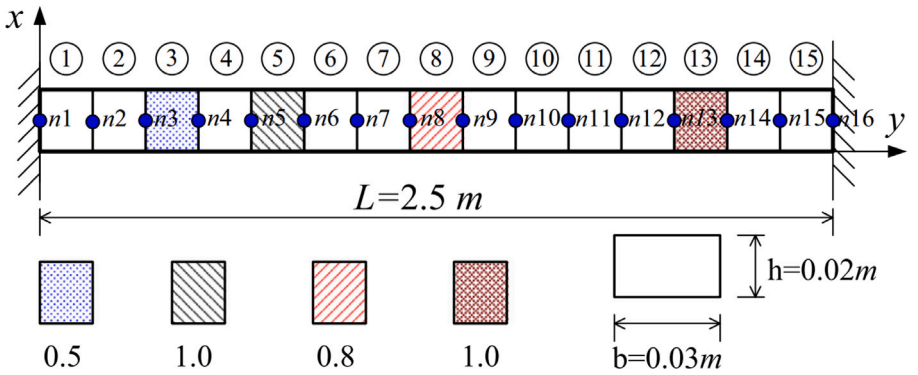

Fig. 3. A clamped–clamped beam [57].

4.1. Case study I: Clamped-clamped beam

The finite element (FE) model of a clamped–clamped beam with 15 elements and 16 nodes pictured in Fig. 3, is established based on Euler–Bernoulli beam theory. The mass density and elasticity modulus are 7810 $\mathrm{kg/m^3}$ and 210 GPa, respectively. The assigned exact stiffness coefficients to elements 3, 5, 8, and 13 are respectively $\theta_1 = 0.5$, $\theta_2 = 1.0$, $\theta_3 = 0.8$, $\theta_4 = 1.0$, as illustrated in Fig. 3. In the context of model updating, those coefficients are taken as uncertain parameters: $\theta = \{\theta_1, \theta_2, \theta_3, \theta_4\}^{\mathrm{T}} \in \mathbb{R}^{4\times 1}$, and need to be updated to make the model fit to the observed modal data $\mathcal{D}$. In this example, the first six natural frequencies and mode shapes are considered to update the model. For simplicity, this example neglects any noise error.

The improved ABC-NS sampler and the original one are now employed by considering uniform priors over the stiffness coefficients to be updated varying between 0.3 and 1.2. The stopping criterion is defined when the difference between two successive tolerance threshold values falls below 10^{-9}. Fig. 4 shows the convergence of the updated stiffness coefficients towards the exact values over the populations for both samplers. The inferred values show a wider spread at the start of the first populations, but this narrows over the iterations and the mean value converges surely to the exact values throughout after 49 iterations with the improved sampler while 63 iterations are required to ensure convergence with the original ABC-NS sampler. Both samplers successfully provide good estimates of the exact values.

Fig. 5 shows on a logarithmic scale the convergence histories, giving the evolution of the discrepancy function values over the iterations. One can see that the improved ABC-NS sampler can bring down the number of iterations required for convergence. In

Algorithm 3 Improved ABC-NS sampler for parameter estimation and model selection

Input: Given a set of observations $\mathcal{D}$, a set of possible models $\{\mathcal{M}_1, \mathcal{M}_2, \dots, \mathcal{M}_\kappa\}$, a tolerance threshold ε_1, a discrepancy metric $\rho(\bullet)$, a set of hyperparameters (α_0, β_0), a number of iterations $t_{\max}$
At iteration $t = 1$
for $i = 1, \dots, \mathrm{N}$ **do**
  repeat
    Draw $\mathcal{M}^*$ from the prior $\mathbb{P}(\mathcal{M})$
    Sample θ^* from the prior $\mathbb{P}(\theta|\mathcal{M}^*)$
    Simulate a candidate data set $\mathcal{D}_s \sim f(\cdot|\theta^*, \mathcal{M}^*)$
    Compute $\rho_i^{(1)} = \rho(\mathcal{D}, \mathcal{D}_s)$
  until $\rho(\mathcal{D}, \mathcal{D}_s) \leq \varepsilon_1$
  Store $\mathcal{M}_i^{(1)} = \mathcal{M}^*$, $\theta_i^{(1)} = \theta^*$, $\rho_i^{(1)} = \rho(\mathcal{D}, \mathcal{D}_s)$
end for
Store the first population $\mathcal{P}^{(1)} = (\mathcal{M}^*, \theta^*)$
Compute the sample weight $\psi_i^{(1)} = \frac{1}{\varepsilon_1}\left(1 - \left(\frac{\rho_i^{(1)}}{\varepsilon_1}\right)^2\right), \quad i = 1, \dots, \mathrm{N}$
Sort $\rho_i^{(1)}$ in descending order and store them.
Compute the next tolerance threshold $\varepsilon_2 = \rho_{\alpha_0 \mathrm{N}}^{(t)}$
Drop particles with $\rho_i^{(1)} \geq \varepsilon_2, \quad \{\psi_k\}_{k=1}^{\alpha_0 \mathrm{N}} = 0$ ▷ A weight of zero is assigned to the dropped particles
Normalise the weights so that $\sum_{\ell=1}^{(1-\alpha_0)\mathrm{N}} \psi_\ell^{(1)} = 1$
Select $\beta_0 \mathrm{N}$ particles from the remaining based on the weights and store the pair $(\mathcal{M}^*, \theta^*) \in \mathcal{A}^{(1)}$
For each model, define the ellipsoid by its centre of the mass and covariance matrix $\mathcal{E}_k^{(1)} = \{\mu_k^{(1)}, C_k^{(1)}\}$, $k = 1, \dots \kappa$ ▷ The covariance matrix $C_k^{(1)}$ is obtained by multiplying the covariance matrix $\mathbf{A}$ by a shrinking factor G For all $2 \leq t \leq t_{\max}$
for $t = 2, \dots, t_{\max}$ **do**
  for $j = 1, \dots, (1 - \beta_0)\mathrm{N}$ **do**
    repeat
      Sample $\mathcal{M}^*$ from the prior $\mathbb{P}(\mathcal{M})$ ▷ updated the priors on the models through the populations
      Sample θ^* inside the ellipsoid $\mathcal{E}_*^{(t-1)}$
      Simulate a candidate data set $\mathcal{D}_s \sim f(\cdot|\theta^*, \mathcal{M}^*)$
      Compute $\rho_i^{(1)} = \rho(\mathcal{D}, \mathcal{D}_s)$
    until $\rho(\mathcal{D}, \mathcal{D}_s) \leq \varepsilon_t$
    Store $\mathcal{M}_j^{(t)} = \mathcal{M}^*$ and $\theta_j^{(t)} = \theta^* \in S^{(t)}$
  end for
  Get the next population, $\mathcal{P}^{(t)} = \mathcal{A}^{(t-1)} \cup S^{(t)}$ with their correspondent distance value $\rho^{(t)}$
  Sort $\rho^{(t)}$ and define $\varepsilon_{t+1} = \rho_t^{(\alpha_0 \mathrm{N})}$
  Compute new weights for all particles as in line (13) and normalise them
  Define the new set of alive particles $\mathcal{A}^{(t)}$ as in line (18)
  Update the hyper-parameters of the ellipsoids using $\mathcal{A}^{(t)}$, $\mathcal{E}^{(t)} = \{\mu_k^{(t)}, C_k^{(t)}\}, \quad k = 1, \dots, \kappa$ ▷ The covariance matrix is obtained in the same way as in line (19)
end for
Output: Posterior model probabilities, Marginal distributions

addition, the improved sampler converges to a set of samples in a region with even the lowest discrepancy function values compared with the original sampler as one can see from the same figure.

Fig. 6(a) and (b) show scatter plots and the marginal posterior distributions of the updated stiffness coefficients obtained from the last population. One can see that the posterior samples were concentrated in a smaller range, leading to a peaked posterior PDF well centred around the exact values. Each histogram has a clear peak, where the orange dashed lines in the plots on the diagonal direction are the identified mean values of the posterior distributions of stiffness coefficients. The lower and upper triangular matrices are the contour plots and scatter plots, respectively, given a pair of coefficients. Overall, one can see that stiffness coefficients are well identified as the exact values.

Fig. 7 displays the updated samples from the improved ABC-NS sampler over some intermediate populations uniformly drawn from the prior distribution in the range of [0.3 – 1.2]. One can see how the particles evolve progressively towards the relevant regions of the parameter space by decreasing gradually the tolerance-threshold values. From the last population, one can see how the obtained posterior samples are concentrated around the exact value (depicted by the large circle).

Fig. 8 shows a comparison between the posterior samples obtained from the last population for both samplers and how they are enclosed in an ellipsoids following the COV and MVEE approaches. One can see how the posterior particle sets obtained from

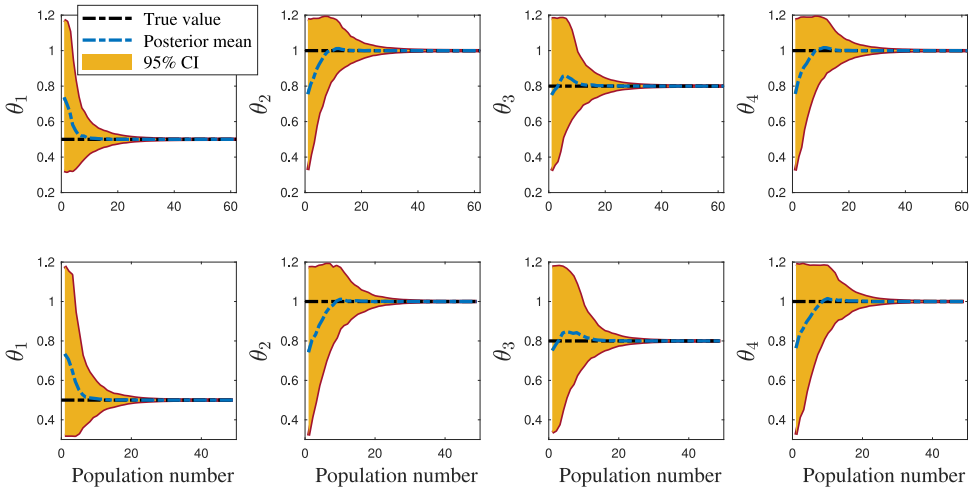

Fig. 4. Evolution of the mean values of the unknown stiffness coefficients over the populations obtained from the original ABC-NS sampler (on the top), and the improved ABC-NS sampler (on the bottom).

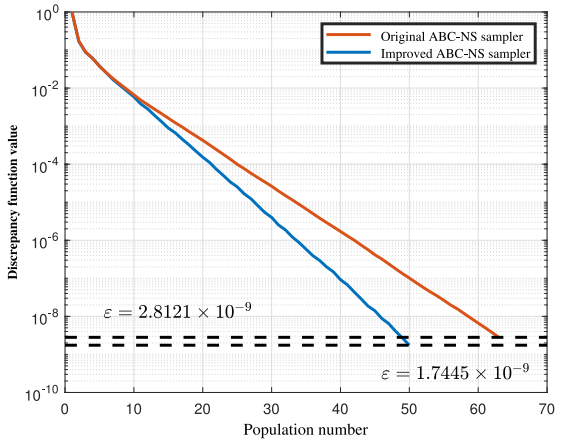

Fig. 5. Convergence histories of the discrepancy function using the original and improved ABC-NS samplers.

Table 1
Comparison between both samplers: computation time and model evaluations.

Sampler	Computation time (s)	Model evaluations
Original ABC-NS sampler	36.7172	49 011
Improved ABC-Sampler	14.7103	21 805

the improved sampler are more compact and concentrated in a smaller region compared with the ones obtained from the original sampler.

Finally, Table 1 shows a comparison between both samplers in terms of computational time and model evaluations. One can see a significant reduction in the computational time with a reduction in the number of model evaluations required for the inference process.

4.2. Case study II: 2-D truss structure

4.2.1. ABC-NS for model updating

The 25-bar planar truss pictured in Fig. 9 is considered as the second numerical example. The FE model of the structure is defined using planar 2-nodes truss elements and has 12 joints leading to a total of 21 degrees of freedom. The mass density and the modulus of elasticity of the material are defined as 7500 $\mathrm{kg/m^3}$ and 210 GPa, respectively. All the elements of the structure are defined with a cross-section area of 18 $\mathrm{cm^2}$. To discretise the mode shapes, five sensors monitoring x and y-directions are defined at nodes n_2,

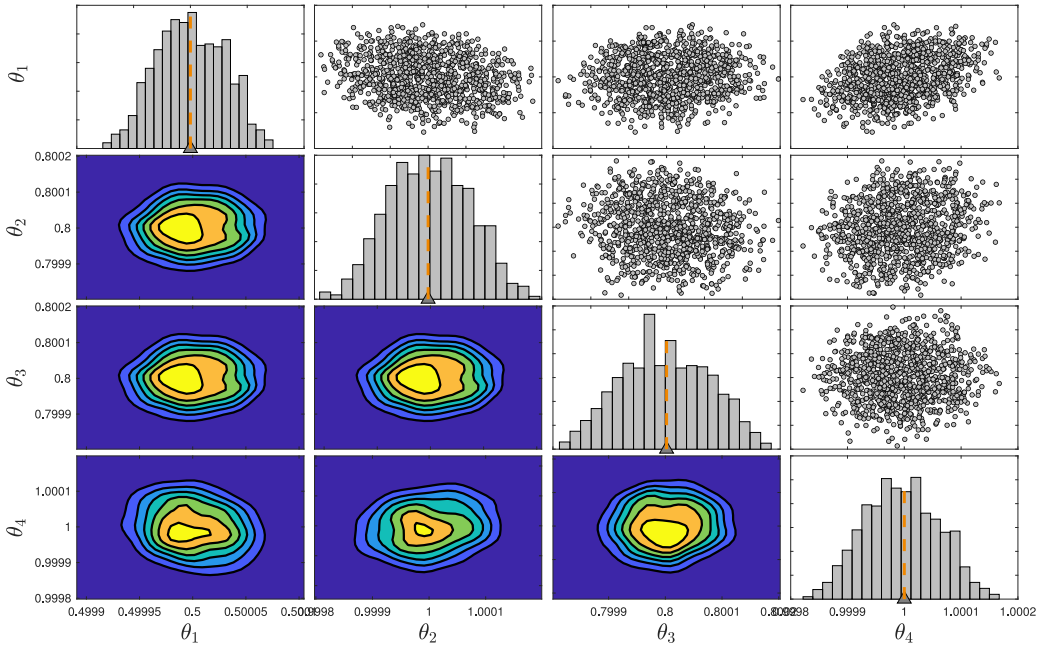

(a) Improved ABC-NS sampler

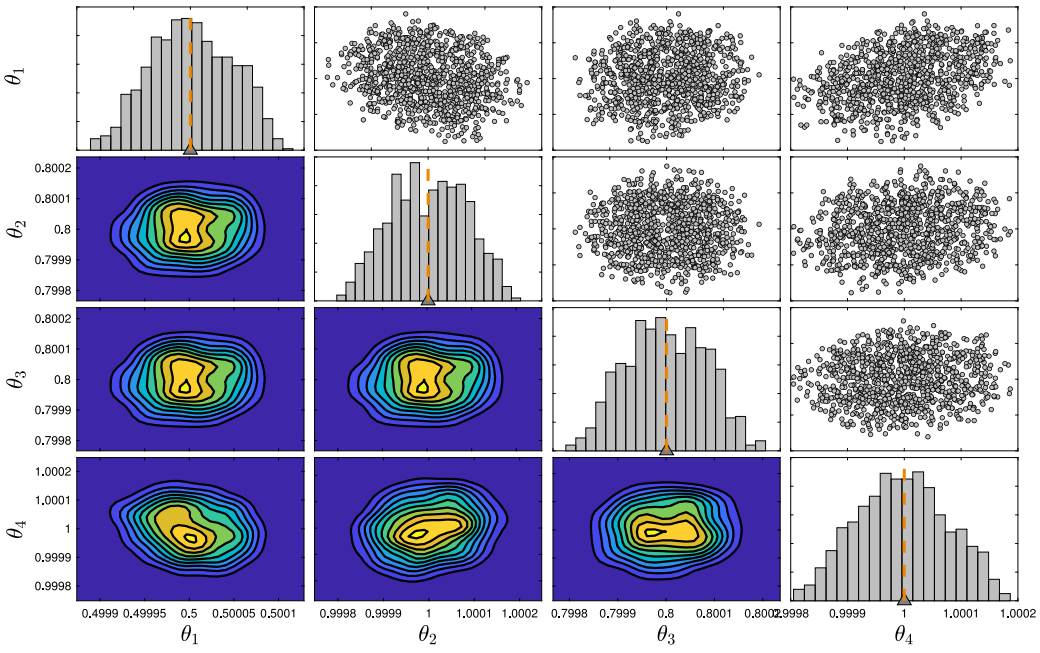

(b) Original sampler

Fig. 6. Probabilistic inference of the unknown stiffness coefficients using both samplers.

n_4, n_6, n_9 and n_{11} as indicated with red arrows in Fig. 9. The first eight frequencies and mode shapes are considered in this example as the measured data. The performance of the improved ABC-NS sampler is further studied by considering different noise levels.

First, model updating is conducted in order to compare the samplers in terms of computational efficiency and accuracy. The unknown parameters to be updated in this example are the stiffness coefficients of 15 bars randomly selected for the purpose of this study. Those bars are numbered in the model as follows:

$$\{⑨\ ③\ ⑯\ ⑰\ ⑦\ ⑪\ ⑥\ ㉒\ ⑭\ ④\ ②\ ⑩\ ⑤\ ⑳\ ㉑\}$$

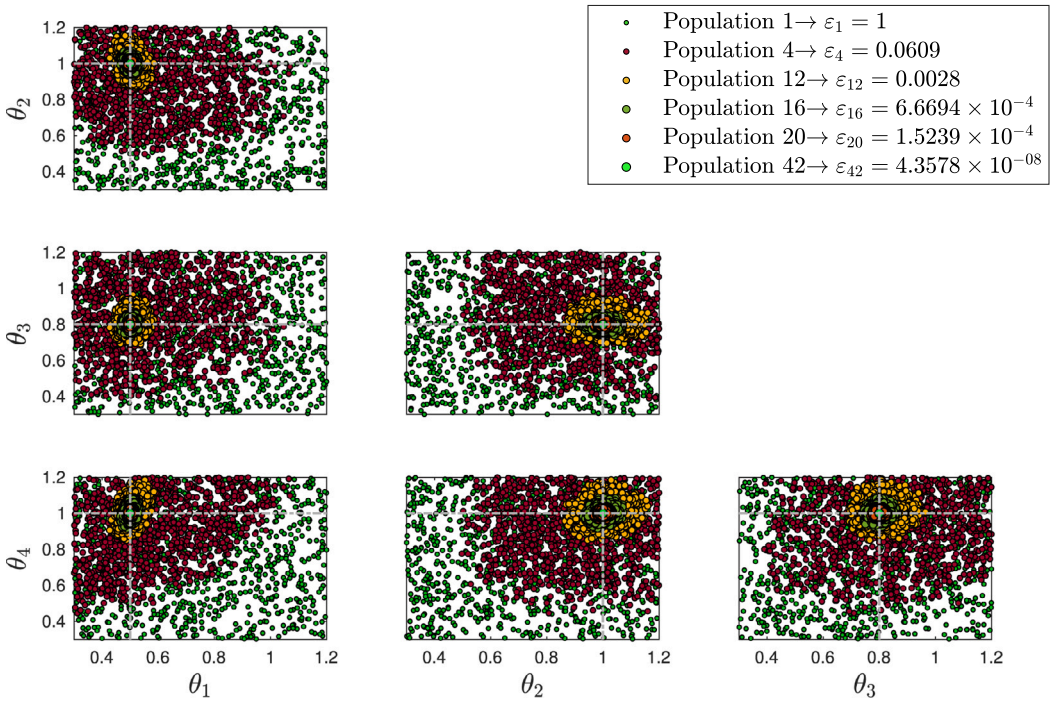

Fig. 7. Evolution of the posterior samples over some selected populations using the improved ABC-NS sampler. The light grey lines indicate the respective exact values.

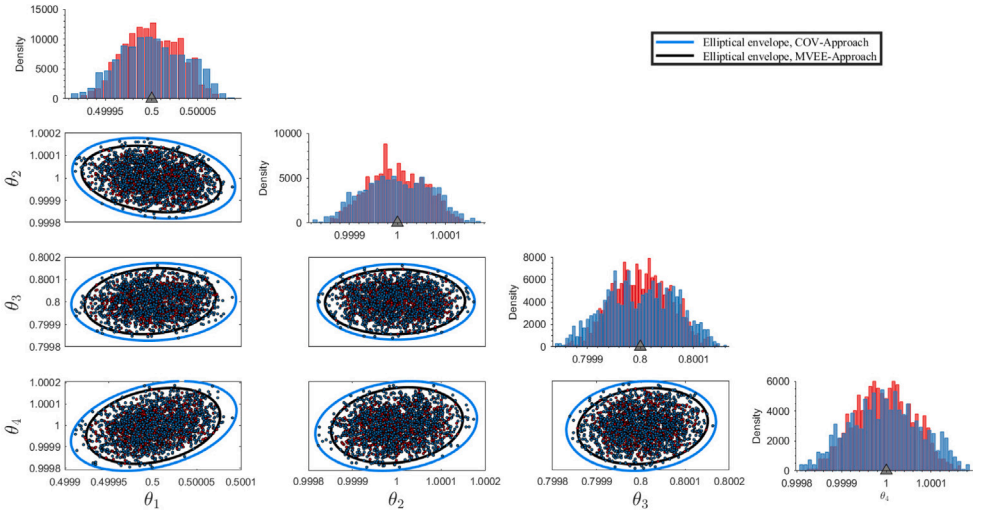

Fig. 8. Posterior samples obtained from the final population enclosed an ellipsoids using the original and improved ABC-NS samplers.

The assigned exact values of the 15 stiffness coefficients are given in the third column of Table 2. The prior distribution of each of the 15 unknown parameters is assumed to be uniformly distributed over the identical interval [0.3 – 1.2]. To implement the improved ABC-NS sampler, the hyperparameters were set as in the first example.

Table 2 shows the obtained results from the last population for the different noise levels. It can be seen from the fourth column that for noise-free case, all the updated stiffness coefficients are identical to the exact values revealing an outstanding performance of the novel sampler, the errors for all the stiffness coefficients presented in the fifth column are small; the maximum error of 0.5552×10^{-3} is observed. The estimated mean values of the updated samples for the first noise level ($e_\omega = 1\%, e_\varphi = 5\%$) are listed in the sixth column. The errors between the estimated means of the updated samples and the exact values are given in the seventh column, which are less than 2% except for θ_{14}, indicating that the algorithm can provide excellent predictions even when the data are polluted. For the second noise level ($e_\omega = 1\%, e_\varphi = 10\%$), it can be seen from the eighth and ninth columns that the performance

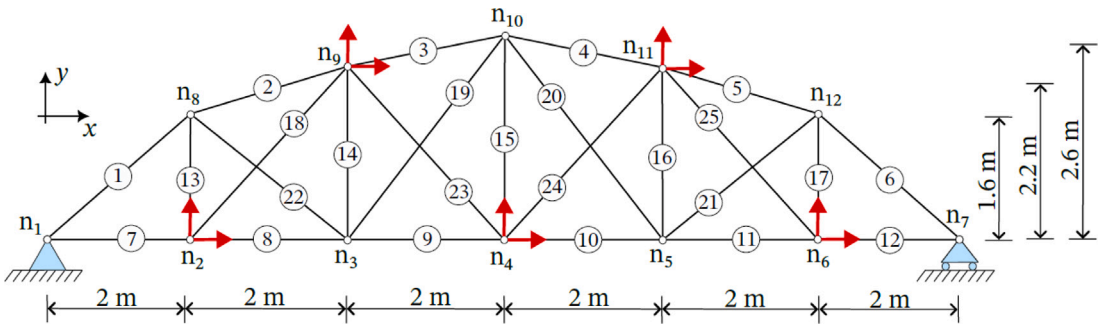

Fig. 9. 2-D Truss structure (red arrows indicate the position and direction of the sensors) [58].

Table 2
Updated stiffness coefficients for different noise levels using the improved ABC-NS sampler.

Bar No.	Parameter	Exact	Noise-free		Level 1		Level 2	
			Mean	Error[a] (%)	Mean	Error (%)	Mean	Error (%)
⑨	θ_1	0.95	0.95	0.1077×10^{-3}	0.9458	0.4401	0.9588	0.9217
③	θ_2	0.90	0.90	0.1069×10^{-3}	0.8963	0.4091	0.9019	0.2072
⑯	θ_3	0.95	0.95	0.0446×10^{-3}	0.9552	0.5448	0.9346	1.6208
⑰	θ_4	0.87	0.87	0.0459×10^{-3}	0.8721	0.2451	0.8683	0.1991
⑦	θ_5	1.00	1.00	0.3678×10^{-3}	1.0045	0.4517	0.9645	3.5502
⑪	θ_6	1.00	1.00	0.1208×10^{-3}	0.9964	0.3571	1.0061	0.6111
⑥	θ_7	0.90	0.90	0.1262×10^{-3}	0.8975	0.2765	0.9002	0.0271
㉒	θ_8	0.92	0.92	0.1101×10^{-3}	0.9256	0.6040	0.9160	0.4307
⑭	θ_9	1.00	1.00	0.1175×10^{-3}	0.9997	0.0318	0.9936	0.6394
④	θ_{10}	1.00	1.00	0.1439×10^{-3}	1.0025	0.2495	1.0005	0.0520
②	θ_{11}	0.85	0.85	0.0927×10^{-3}	0.8584	0.9844	0.8327	2.0316
⑩	θ_{12}	1.00	1.00	0.0088×10^{-3}	1.0031	0.3055	0.9901	0.9938
⑤	θ_{13}	0.95	0.95	0.1553×10^{-3}	0.9506	0.0592	0.9427	0.7722
⑳	θ_{14}	0.93	0.93	0.5446×10^{-3}	0.9609	3.3178	0.9187	1.2160
㉑	θ_{15}	0.90	0.90	0.5552×10^{-3}	0.8903	1.0822	0.9029	0.3231

[a] Error $= \frac{|\theta_{\text{Exact}} - \theta_{\text{predicted}}|}{\theta_{\text{Exact}}}$.

of the improved ABC-NS sampler is still good and acceptable, the errors between the exact and predicted stiffness coefficients are less than 4% at the worst case (for Bar 7), which demonstrates the robustness and efficiency of the improved ABC-NS sampler to deal with model updating.

Fig. 10 shows the posterior probability distributions of the unknown stiffness coefficients obtained from the last population. One can see that the PDFs are well peaked on the exact values with small uncertainty. The improved sampler recovers perfectly well the real values. Fig. 11 shows the same results by considering noisy modal data using Level 1 from where one obtains a peaked posterior PDFs with small uncertainty. Finally, it is worth mentioning that the original sampler provides good estimates of the exact values, not shown here for brevity.

Next, both samplers are compared in terms of computational efficiency and accuracy. To this end, the number of iterations required to achieve convergence will be compared, which is reported in terms of number of populations. Fig. 12 shows the convergence histories of the discrepancy function in log-scale for both samplers. Again, one can see a remarkable performance of the improved sampler, more pronounced for high-dimensional problems. Clearly the inclusion of the MVEE has significantly improved the computational efficiency and convergence speed. The value of the top of the dashed line is the final tolerance value achieved during the inference process. One can see that the new sampler allows to reach a region in which the posterior samples have smaller discrepancy values meaning a better agreement with the observed data. Additionally, the impact of the shrinking value G on the convergence speed is investigated. One can see from the same figure that when the G value is equal to 1, the number of iterations required for convergence is increased to 191.

The accuracy of the novel sampler is evaluated quantitatively via the Closeness Index (CI) [59,60]. The CI compares the predicted stiffness coefficients with the exact values as follows:

$$\text{CI} = 1 - \frac{\|\theta_{\text{Exact}} - \theta_{\text{Predicted}}\|}{\|\theta_{\text{Exact}}\|} \quad \text{for} \quad 0 \leq \text{CI} \leq 1 \tag{19}$$

where θ_{Exact} and $\theta_{\text{Predicted}}$ represent the exact and predicted stiffness coefficient vectors, respectively. The closer a value of CI to 1 indicates a better prediction capability.

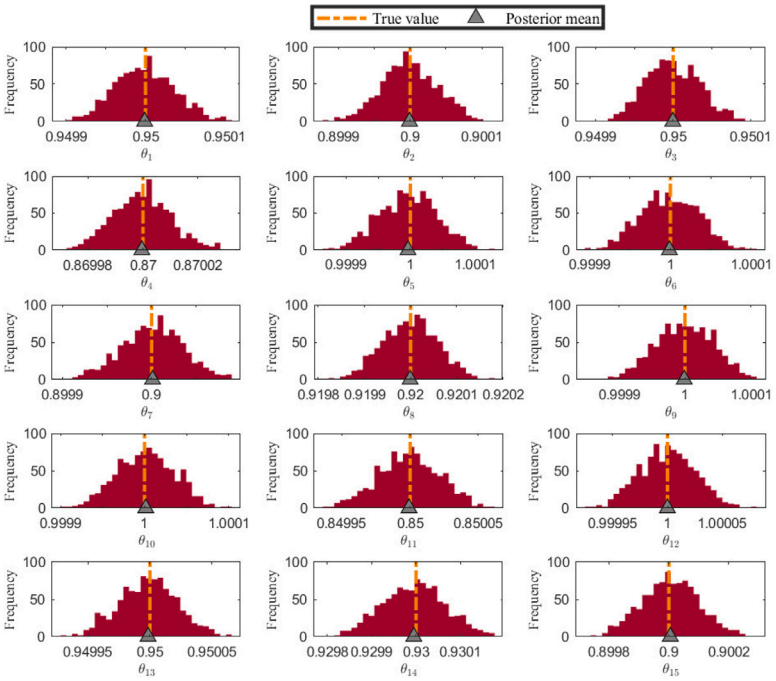

Fig. 10. Posterior distributions (histograms) of the predicted stiffness coefficients obtained from the last population (free-noise data).

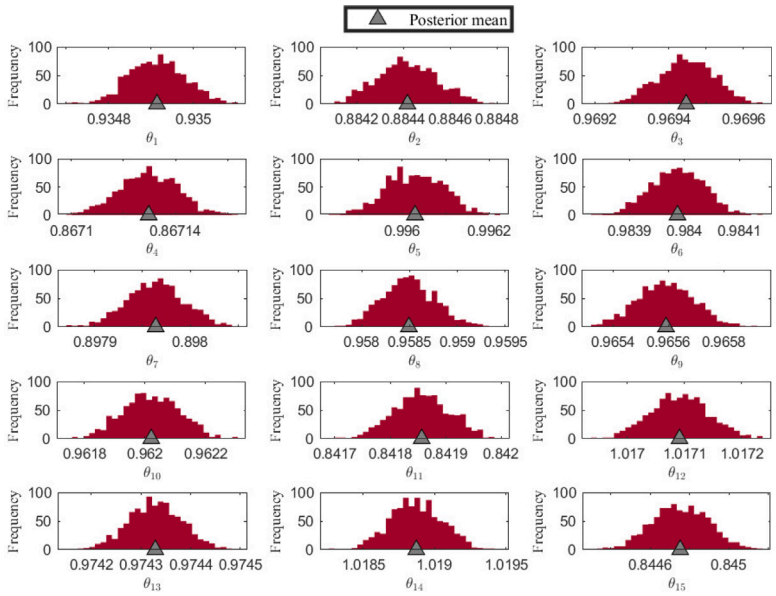

Fig. 11. Posterior distributions (histograms) of the predicted stiffness coefficients obtained from the last population (noisy data).

The CI compared in Fig. 13 confirms the performance of the improved sampler. One can see that the improved sampler reaches the value of 1 more quickly meaning a better convergence speed towards the highest probability region compared with the original sampler. The CI shows that both samplers provide good predictions (as CI → 1) with a clear advantage of the improved sampler in terms of computational efficiency. Clearly the inclusion of the MVEE technique boosts the ABC-NS sampler without compromising the accuracy of the posterior estimates.

In order to make a comparison between the improved ABC-NS sampler and a likelihood-based sampler, the transitional Markov chain Monte Carlo (TMCMC) method [11] which belongs the class of the sequential particle filter methods [61] has been chosen as

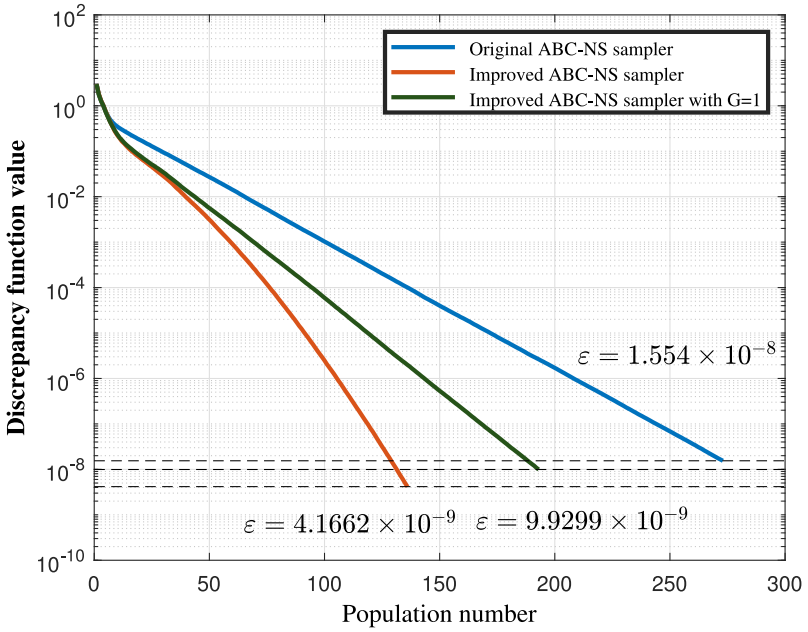

Fig. 12. Convergence histories of the discrepancy function using the original and improved ABC-NS samplers.

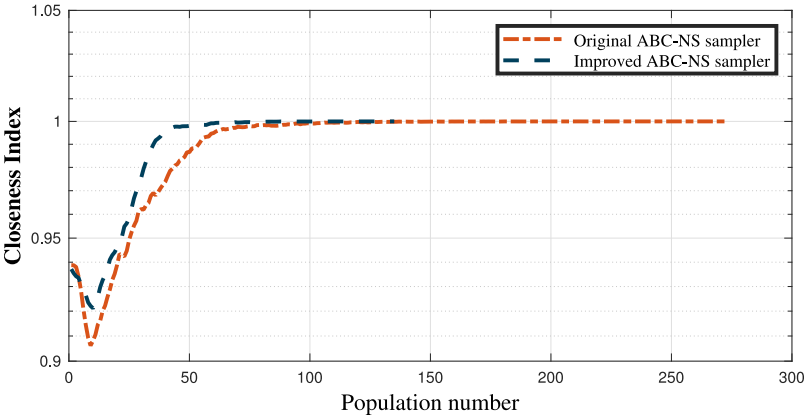

Fig. 13. Comparison between the computational accuracy and efficiency (free-noise data).

it is widely used in the literature. The TMCMC settings was done following [62] and the results are summarised in Table 3. Overall both samplers provide good predictions.

4.2.2. ABC-NS for model selection and damage detection

To assess the effectiveness of the improved sampler to deal with model selection and structural damage detection, different classes of competing models have been defined based on a preliminary sensitivity analysis reported in Fig. 14 [58]. In this analysis, the stiffness of the bar elements of the structure were sequentially affected by a perturbation of 5%, to obtain the mean sensitivities in terms of frequencies $\overline{S^f}$ across the eight considered modes [58]. The results of the sensitivity study summarised in Fig. 14 guided the definition of different model classes $\{\mathcal{M}_i,\ i = 1, \ldots, 5\}$, incorporating an increasing number of parameters of decreasing sensitivity. Specifically, five different model classes have been defined as depicted in Fig. 15 and Table 4. Note that these model classes represent nested models, wherein each subsequent class includes the parameters of the previous class. The defined competing models are given in Table 4 with the corresponding stiffness coefficients associated to each bar. It is supposed that the stiffness coefficients were unknown and were inferred using the improved ABC-NS sampler. In this example, the lower and upper bounds were 0.3 and 1.2, respectively. The candidate models are parametrised in the same way following the order appearing in the second column in Table 4; for example, for model $\mathcal{M}_1$, θ_1 in the stiffness coefficient is associated to Bar ① while θ_2 is associated to Bar ⑥.

The improved ABC-NS sampler is now employed to deal with model-class selection and calibration of the stiffness coefficients. The hyperparameters were set as in the previous case study. For all the numerical experiments, it is supposed that the candidate

Table 3
A comparison between the updated stiffness coefficients using the improved ABC-NS and TMCMC samplers under noisy modal measurements (Level 1).

Bar No.	Parameter	Exact	Improved ABC-NS sampler		TMCMC	
			Mean	Error[a] (%)	Mean	Error (%)
⑨	θ_1	0.95	0.9458	0.4401	0.9546	0.4836
③	θ_2	0.90	0.8963	0.4091	0.9040	0.4452
⑯	θ_3	0.95	0.9552	0.5448	0.9443	0.6041
⑰	θ_4	0.87	0.8721	0.2451	0.8705	0.0601
⑦	θ_5	1.00	1.0045	0.4517	1.0229	2.2870
⑪	θ_6	1.00	0.9964	0.3571	1.0019	0.1890
⑥	θ_7	0.90	0.8975	0.2765	0.8999	0.0084
㉒	θ_8	0.92	0.9256	0.6040	0.9588	4.2185
⑭	θ_9	1.00	0.9997	0.0318	0.9850	1.4960
④	θ_{10}	1.00	1.0025	0.2495	0.9758	2.4194
②	θ_{11}	0.85	0.8584	0.9844	0.8522	0.2603
⑩	θ_{12}	1.00	1.0031	0.3055	0.9930	0.7012
⑤	θ_{13}	0.95	0.9506	0.0592	0.9488	0.1249
⑳	θ_{14}	0.93	0.9609	3.3178	0.9281	0.2053
㉑	θ_{15}	0.90	0.8903	1.0822	0.8990	0.1079

[a] Error = $\frac{|\theta_{\text{Exact}} - \theta_{\text{predicted}}|}{\theta_{\text{Exact}}}$.

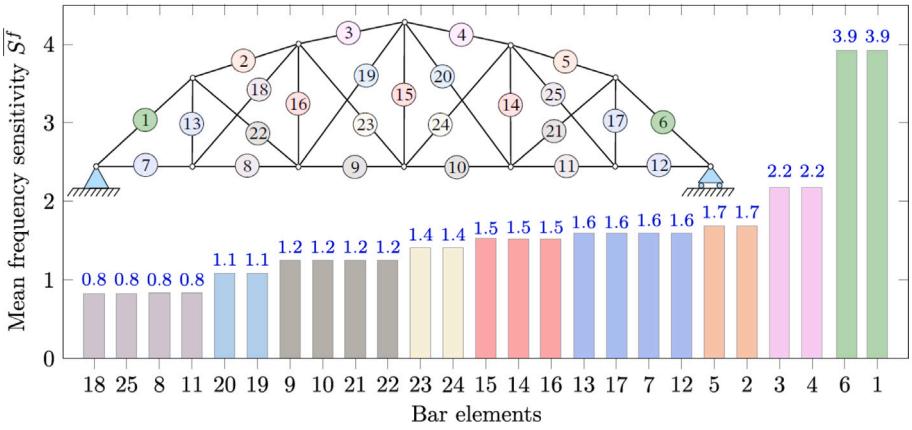

Fig. 14. Sensitivity of the truss structure's bars in terms of frequency.

models are equally probable. To assess the performance of the sampler to recover the true model and to analyse its behaviour, five numerical simulations were run, where in each simulation the true model from where the measured data were generated is changed.

Fig. 16(a)–(e) show the posterior model probabilities (PMPs) obtained over the populations required for convergence. Fig. 16(a) shows the PMPs over the populations where the modal data were simulated from $\mathcal{M}_1$. The algorithm first eliminates overly complex models $\mathcal{M}_4$ and $\mathcal{M}_5$ and leaves $\mathcal{M}_1$, $\mathcal{M}_2$ and $\mathcal{M}_3$ to compete. The algorithm converges to the former models after 70 populations with PMPs of 0.54, 0.32 and 0.16, respectively. When $\mathcal{M}_2$ is the true model, the improved ABC-NS sampler rules out $\mathcal{M}_1$ as it is too simple to explain the observed modal data and converges to the remaining models with a preference to the generative model as shown in Fig. 16(b). When the data were generated from $\mathcal{M}_3$ and $\mathcal{M}_4$, the sampler behaves similarly, it eliminates simpler models and keeps the models that could explain the measured data with a preference for the generative models as illustrated in Fig. 16(c) and (d). In the same way, when the data were simulated from $\mathcal{M}_5$ which has the highest complexity among all models, the sampler eliminates gradually the least likely models following the degree of complexity, and converges surely to the true model with a PMP equal to 1.

To sum up, the sampler converges to the true model from which the data were generated in each case and eliminates progressively the least likely model(s). One can see how the algorithm tends to select simpler models first then, when the model is unable to capture the data, it switches to a more complex models. Clearly the parsimony principle is well embedded in the sampler by favouring models with fewer parameters while maintaining their ability to effectively explain the observed data as previously shown in Refs. [37,63,64] using the ABC method. A comparison between both samplers shows that the improved sampler converges more quicker than the original ABC-NS sampler. The original sampler provides similar results and converges to the true model in each case (not shown for brevity).

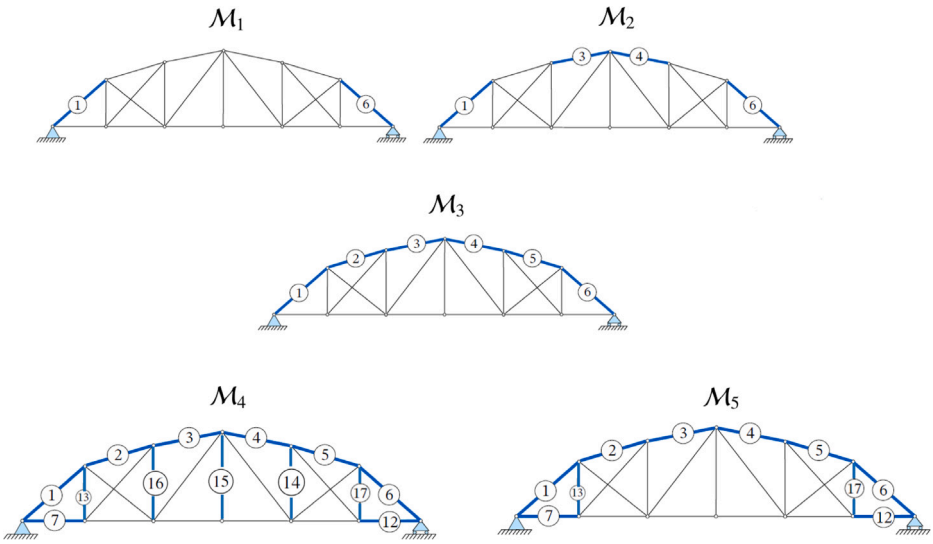

Fig. 15. Definition of the candidate model classes.

Table 4
Candidate model classes defined based on a frequency sensitivity analysis.

Candidate model	Damaged bars	Stiffness coefficient @ bars	Model size
$\mathcal{M}_1$	① ⑥	0.95 @ ⑥ 0.90 @ ①	2
$\mathcal{M}_2$	① ⑥ ④ ③	0.95 @ ⑥ ④ 0.90 @ ① ③	4
$\mathcal{M}_3$	① ⑥ ④ ③ ② ⑤	0.95 @ ⑥ ④ ② 0.90 @ ① ③ 0.85 @ ⑤	6
$\mathcal{M}_4$	① ⑥ ④ ③ ② ⑤ ⑫ ⑦ ⑰ ⑬	0.95 @ ⑥ ④ ② ⑬ ⑰ 0.90 @ ① ③ 0.925 @ ⑫ 0.85 @ ⑤ ⑦	10
$\mathcal{M}_5$	① ⑥ ④ ③ ② ⑤ ⑫ ⑦ ⑰ ⑬ ⑯ ⑭ ⑮	0.95 @ ⑥ ④ ② ⑬ ⑰ 0.90 @ ① ③ ⑯ 0.925 @ ⑫ ⑭ 0.85 @ ⑤ ⑦ ⑩	13

For illustrative purposes, Fig. 17 shows the posterior distributions of the updated stiffness coefficients when the assumed true model is $\mathcal{M}_3$, obtained from the last population. The scatter plots in the upper triangular block represent the samples from the improved ABC-NS sampler at the final stage. The diagonal plane presents the one-dimensional marginalised posterior distributions of the updated stiffness coefficients. As one can see, the posterior uncertainty is very small and the histograms are well peaked on the assumed true values indicated by a dashed orange line. The results are demonstrated only for $\mathcal{M}_3$, which has six parameters to be updated, but similar trends was observed for the other cases.

The computations of the PMPs show some fluctuations because of the stochastic nature of the ABC-NS sampler. To get precise estimates of the PMPs, one replicates the inference scheme 100 times for each case. Fig. 18 depicts the final estimated PMPs obtained from the improved ABC-NS sampler. The final case where $\mathcal{M}_5$ is the true model is not shown because the sampler converges to the true model with a probability equal to 1.

4.3. Case study III: A 25-bar truss structure

This section keeps the same 25-bar truss structure shown in Fig. 9 and revisits the previous case study, while model comparison/selection is performed among models that are not nested inside each other. From this perspective, a "model" is just a possible structural health state/condition of the structure. There is no general model that can reproduce all the different pathologies a structure may present, but instead, specific models could be defined for specific failure mechanisms or assembly and construction defects that have been defined by an experienced user. While in the first two case studies, the damage is simulated by only reducing

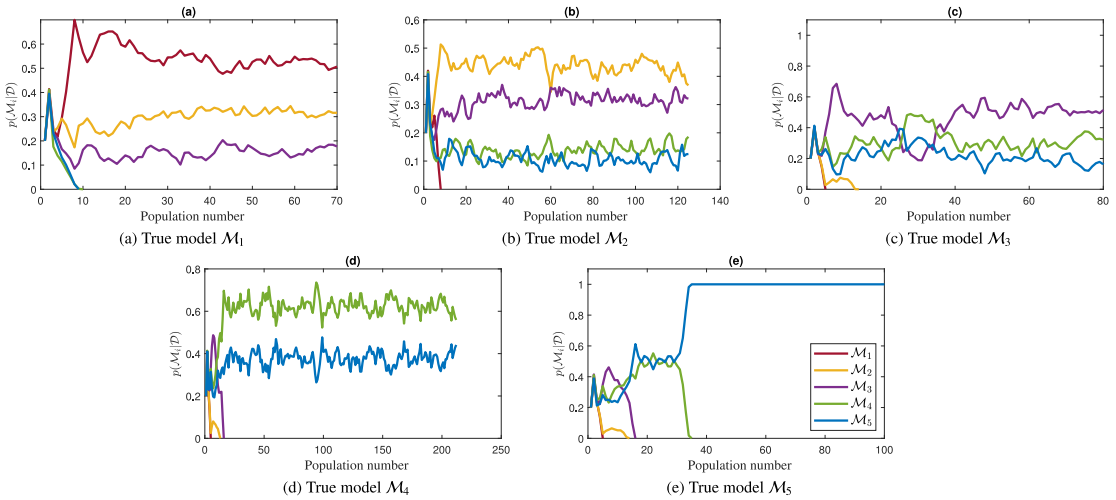

(a) True model $\mathcal{M}_1$ (b) True model $\mathcal{M}_2$ (c) True model $\mathcal{M}_3$

(d) True model $\mathcal{M}_4$ (e) True model $\mathcal{M}_5$

Fig. 16. Evolution of the posterior model probabilities over the populations using the improved ABC-NS sampler.

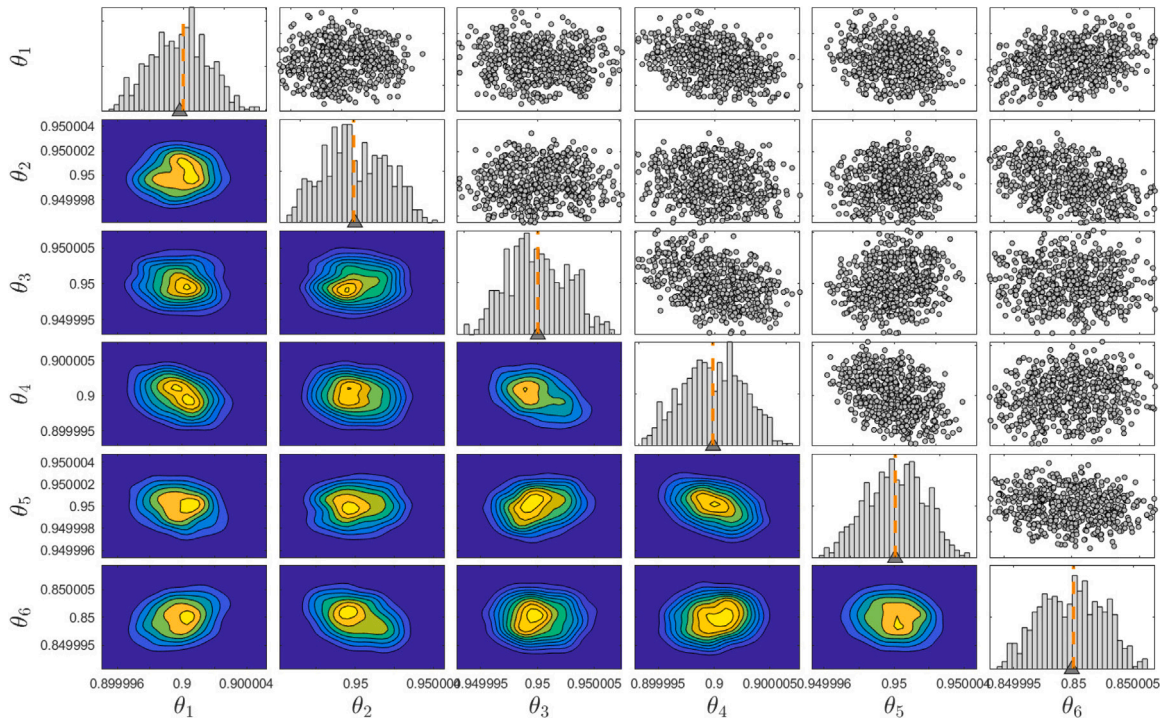

Fig. 17. Probabilistic identification of the unknown stiffness coefficients for model $\mathcal{M}_3$ using the improved ABC-NS sampler.

the elasticity modulus values, in this case, the damage is simulated by reducing the elasticity modulus or the sectional area, meaning the presence of manufacturing flaws at specific locations of the structure. The reduction in the elastic modulus of the members is applied to simulate the assembly defects in the connected joints and imperfect support joints. In the context of this study, five hypothetical models have been designed, in which each model is assumed to mirror a real health state that the structure may experience. The competing models are enumerated in Table 5 with the corresponding number of parameters. For $\mathcal{M}_5$, the fact that the reduction of the sectional area alter the mass and stiffness matrices need to be stressed. For simplicity, the same notation of the model parameters is taken. The same hyperparameters were kept for the improved ABC-NS implementation.

Once the competing models have been defined, the sampler is run to select the most likely model from a set of competing models based on measured modal data. As in the previous example, a model is chosen from which the data were simulated and the sampler is run to see if it is able to recover the true model with the right stiffness coefficients. The competing models are supposed to be

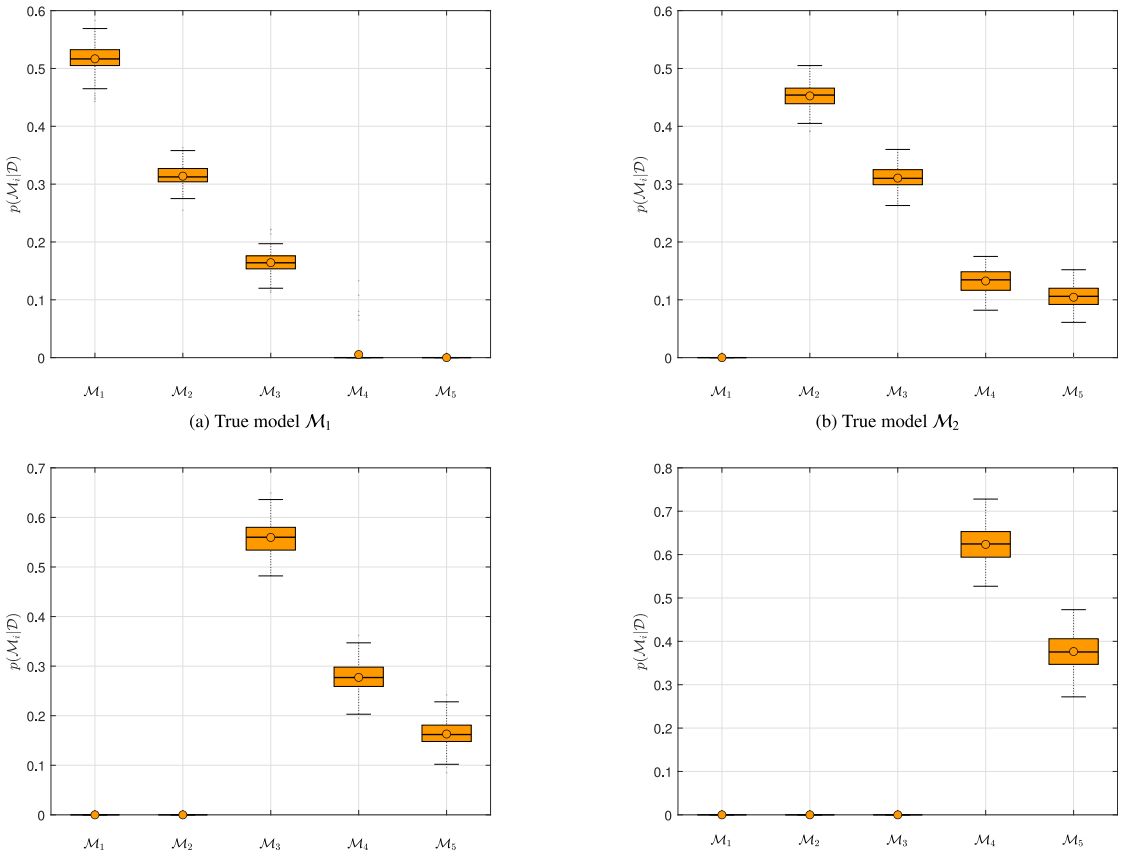

(a) True model $\mathcal{M}_1$ (b) True model $\mathcal{M}_2$

(c) True model $\mathcal{M}_3$ (d) True model $\mathcal{M}_4$

Fig. 18. Box-plots giving the posterior model probabilities using 100 independent replications.

Table 5
Definition of the candidate model classes.

Candidate model	Defect type	Bars	Changes	Model size
$\mathcal{M}_1$	Imperfect support joints n_1	① ⑦	10% reduction in elastic modulus	2
$\mathcal{M}_2$	Imperfect support joints n_7	⑥ ⑫	5% reduction in elastic modulus	2
$\mathcal{M}_3$	Assembly defect in n_3	⑧ ⑨ ⑭ ⑲	5% reduction in elastic modulus	4
$\mathcal{M}_4$	Assembly defect in n_5	⑩ ⑪ ⑳ ㉑	10% reduction in elastic modulus	4
$\mathcal{M}_5$	Manufacturing flaws	⑨ ⑮ ⑲ ㉓	10% reduction in area	4

plausible, that is, each model was considered as equally probable. We precise that 10% reduction in elastic modulus means that the stiffness coefficients for damaged bars are equal to 0.9. Uniform priors were also used for the stiffness coefficients.

Fig. 19 displays the PMPs over the populations. One can see that the algorithm performs very well as it converges towards the right model with a probability equal to 1 in each case. This is because the competing models considered in this example are non-nested in comparison with the former study and the data is noise-free. For a better clarity of the figure, the PMPs are plotted until the sampler converges to the right model with a probability equal to 1. The subsequent iterations are needed to refine the posterior estimates of the stiffness coefficients.

Fig. 20 displays the evolution of the number of particles over the first ten populations until the sampler converges to the model from where the modal data was simulated ($\mathcal{M}_4$ in this case) and eliminates progressively the other competing models. During the inference scheme, the tolerance threshold decreases over the populations and the least likely models are the ones for which their populations die out over the iterations as shown in Fig. 20. To compare both samplers in terms of computational efficiency, Fig. 21 shows the convergence histories for the different scenarios. One can see that the improved ABC-NS sampler is computationally

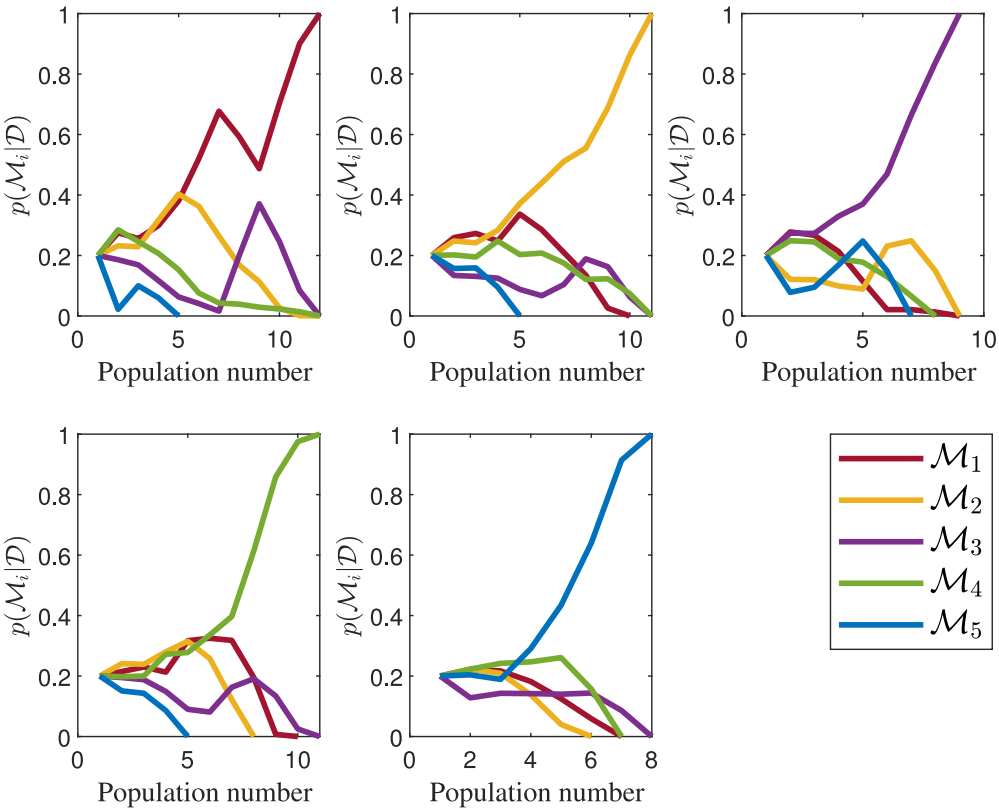

Fig. 19. Evolution of the posterior model probabilities over the populations.

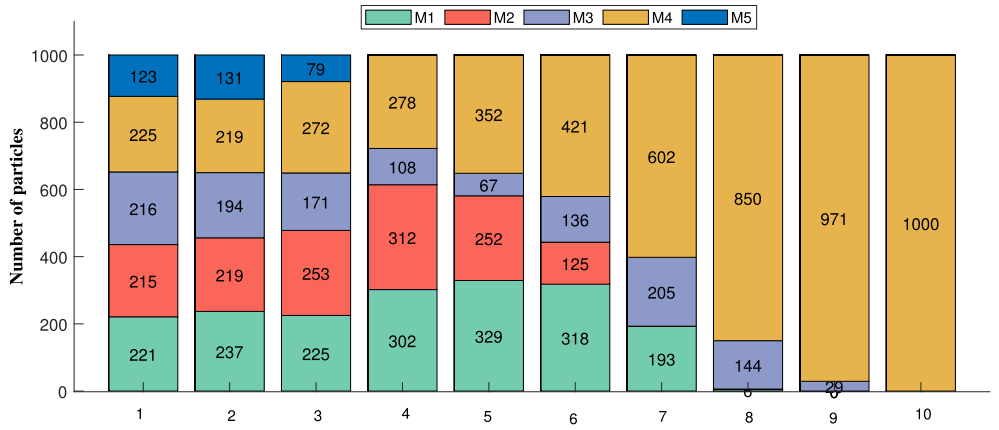

Fig. 20. Evolution of the number of particles over the populations where the true model is $\mathcal{M}_4$.

more efficient than the original ABC-NS sampler since it requires less iterations to ensure convergence, offering the possibility to consider more candidate models to be simultaneously compared and inferred.

For illustrative purposes, the scatter plots are plotted for the cases where the modal data were simulated respectively, from $\mathcal{M}_3$ and $\mathcal{M}_5$. The obtained results are visualised in Fig. 22(a) and (b), showing the correlation and variability of the stiffness coefficients on the upper/lower diagonal plots. Those plots on the main diagonal show the marginal posterior distributions which are Gaussian shaped. The estimated mean values with a dashed line in a orange are effectively indistinguishable from exact values represented by black triangle.

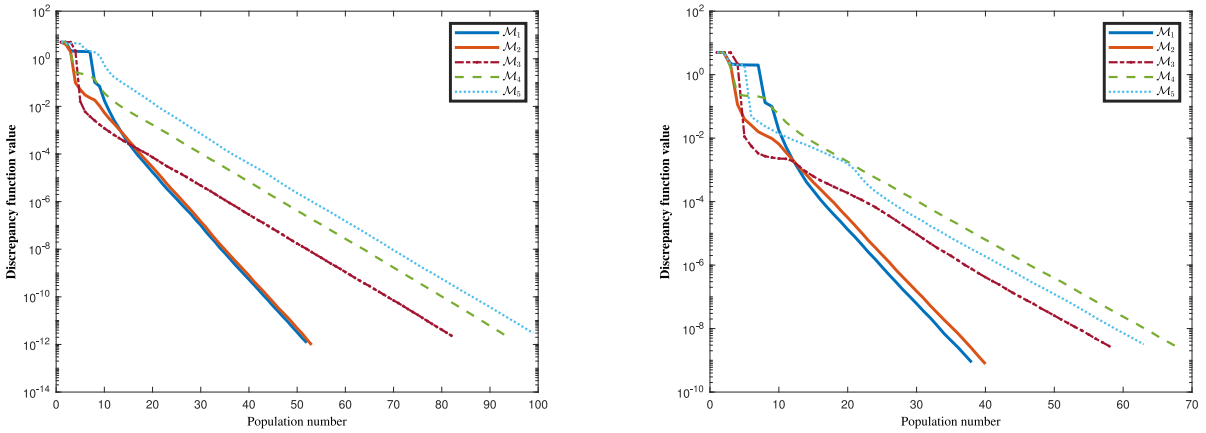

(a) Original ABC-NS sampler (b) Improved ABC-NS sampler

Fig. 21. Comparison between the convergence histories.

Table 6
Noise levels considered in this case study.

Noise level	Frequency and mode shape	
	e_ω (%)	e_φ (%)
1	1	5
2	1	10
3	5	20

Table 7
Updated stiffness coefficients for different noise levels.

Bar No.	Parameter	Exact	Level 1 ($e_\omega = 1\%, e_\varphi = 5\%$)		Level 2 ($e_\omega = 1\%, e_\varphi = 10\%$)		Level 3 ($e_\omega = 5\%, e_\varphi = 20\%$)	
			Mean	Error (%)	Mean	Error (%)	Mean	Error (%)
(10)	θ_1	0.9	0.9007	0.0761	0.9019	0.2126	0.8991	0.0992
(11)	θ_2	0.9	0.9042	0.4720	0.9031	0.3407	0.9104	1.1598
(20)	θ_3	0.9	0.9070	**0.7761**	0.8913	**0.9662**	0.9772	**8.5754**
(21)	θ_4	0.9	0.9028	0.3096	0.8964	0.4022	0.9287	3.1885

4.4. Noise effects

Finally, the focus is on the impact of noise. To do this, it is supposed that the true model from which the data was generated is $\mathcal{M}_4$. Different noise levels have been considered in order to check the effects on the PMPs and also on the posterior estimates. For the considered noise levels illustrated in Table 6, one can see from Fig. 23 that the improved ABC-NS sampler converges to the true model. For a better visualisation, the evolution of the PMPs over the iterations are shown until they reach the value of 1 for the first time. From the last population, the stiffness coefficients considering all the scenarios are recovered. The posterior estimates are summarised in Table 7 from which one can see that even when the modal data is contaminated by noise, the sampler is able to recover accurately the model parameters. The largest error value is less than 10%-observed for Level 3 (for bar (20))).

5. Conclusions

This paper introduced an improved ABC-NS sampler as a new alternative to deal with model updating and model selection applied to structural health monitoring. The numerical experiments show that the ABC-NS sampler coupled with an elegant ellipsoidal nested sampling technique using the concept of *minimum-volume enclosed ellipsoid* (MVEE) can provide worthwhile improvements to sample-efficiency over the earlier ABC-NS sampler. By using the MVEE, the sampler has the ability to draw promising particles

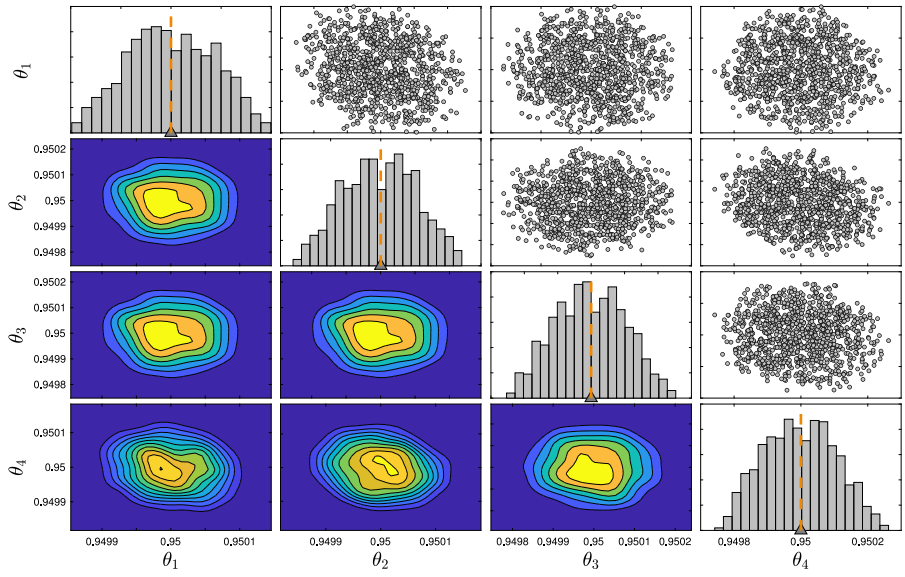

(a) True model $\mathcal{M}_3$

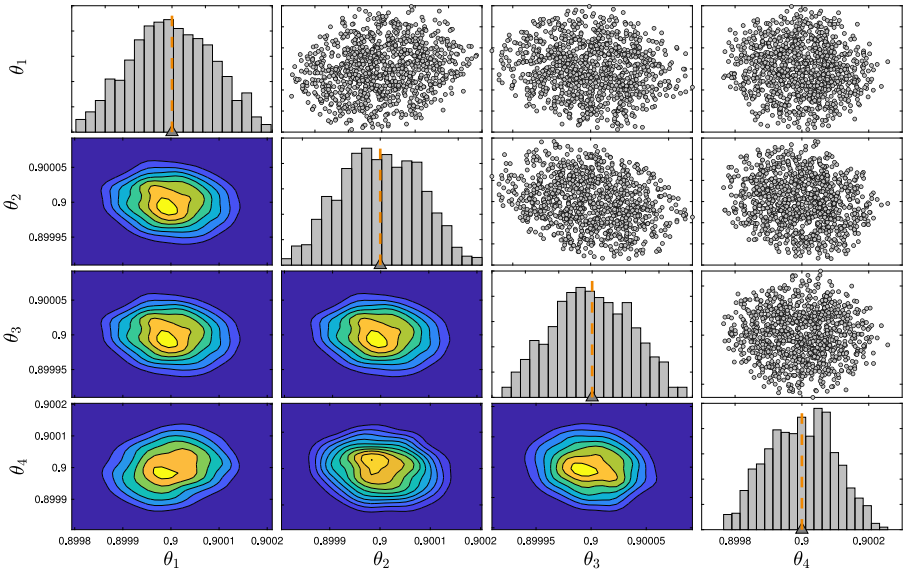

(b) True model $\mathcal{M}_5$

Fig. 22. Probabilistic inference of the stiffness coefficients using the improved ABC-NS sampler.

that are more likely to produce simulated data that provide a better agreement with the measured data. The resulting sampler is conceptually simple, adaptable and gives from the last population a full characterisation of the uncertainties associated to the unknown model parameters in a reasonable computational time. In addition, it has the ability to straightforwardly discriminate between a set of competing plausible models/hypotheses giving to practitioners an all-in-one procedure of both model updating and model selection as opposed to the conventional Bayesian approach.

The application of the improved ABC-NS sampler could be extended to other disciplines and inference problems because of its versatility and adaptability. Future studies should include experimental and field data collected in changing operational conditions, to further validate the effectiveness of the proposed model updating and model selection procedure in realistic scenarios.

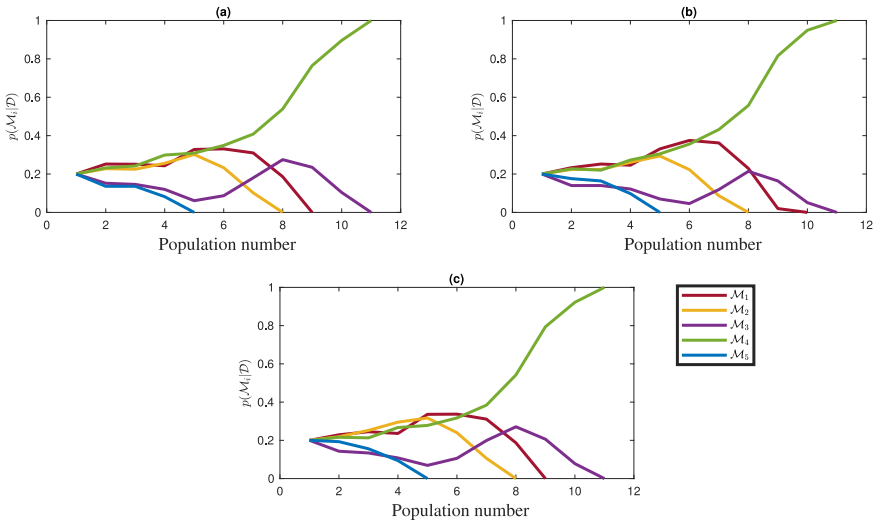

Fig. 23. Evolution of the PMPs over the populations when the modal data is contaminated by noise.

CRediT authorship contribution statement

A. Ben Abdessalem: Writing – original draft, Visualization, Validation, Methodology, Conceptualization. **N. Dervilis:** Visualization, Validation, Methodology, Conceptualization. **D. Wagg:** Visualization, Validation, Methodology, Conceptualization. **K. Worden:** Visualization, Validation, Methodology, Conceptualization.

Code availability

- On acceptance, all the source codes to reproduce the results in this study will be made available to the public on GitHub by the corresponding author.

Declaration of competing interest

The authors certify that they have no conflict of interest to declare.

Data availability

Data will be made available on request.

References

[1] Bi Sifeng, M. Beer, S. Cogan, J. Mottershead, Stochastic model updating with uncertainty quantification: An overview and tutorial, Mech. Syst. Signal Process. 204 (2023) 110784.
[2] Z.Z Zhang, C. Sun, Structural damage identification via physics- guided machine learning: a methodology integrating pattern recognition with finite element model updating, Struct. Health Monit. 20 (4) (2021) 1675–1688.
[3] S. Das, P. Saha, Structural health monitoring techniques implemented on IASC–ASCE benchmark problem: a review, J. Civ. Struct. Heal. Monit. 8 (4) (2018) 689–718.
[4] M. Friswell, J.E. Mottershead, Finite Element Model Updating in Structural Dynamics, Vol. 38, Springer Science & Business Media, 2013.
[5] W.R. Gilks, S. Richardson, D. Spiegelhalter, Markov Chain Monte Carlo in Practice, Chapman and Hall/CRC, 1995.
[6] J.L. Beck, S.-K. Au, Bayesian updating of structural models and reliability using markov chain monte carlo simulation, J. Eng. Mech. 128 (2002) 380–391.
[7] S.H. Cheung, S. Bansal, A new gibbs sampling based algorithm for bayesian model updating with incomplete complex modal data, Mech. Syst. Signal Process. 92 (2017) 156–172.
[8] E. Zhang, P. Feissel, J. Antoni, Bayesian model updating with consideration of modeling error, Eur. J. Comput. Mech. 19 (2010) 255–266.
[9] E.L. Zhang, P. Feissel, J. Antoni, A comprehensive bayesian approach for model updating and quantification of modeling errors, Probab. Eng. Mech. 26 (2011) 550–560.
[10] E. Zhang, J.D. Chazot, J. Antoni, M. Hamdi, Bayesian characterization of young's modulus of viscoelastic materials in laminated structures, J. Sound Vib. 332 (2013) 3654–3666.
[11] J. Ching, Y.C. Chen, Transitional Markov chain Monte Carlo method for Bayesian model updating, model class selection, and model averaging, J. Eng. Mech. 133 (7) (2007) 816–832.
[12] W. Betz, I. Papaioannou, D. Straub, Transitional Markov chain monte carlo: observations and improvements, J. Eng. Mech. 142 (5) (2016) 04016016.

[13] P. Angelikopoulos, C. Papadimitriou, P. Koumoutsakos, X-TMCMC: Adaptive kriging for Bayesian inverse modeling, Comput. Methods Appl. Mech. Eng. 289 (2015) 409–428.
[14] S. Wu, P. Angelikopoulos, C. Papadimitriou, P. Koumoutsakos, Bayesian annealed sequential importance sampling: an unbiased version of transitional Markov chain Monte Carlo, ASCE-ASME J. Risk Uncertain Eng. Syst. Part B Mech. Eng. 4 (1) (2018).
[15] D. Straub, I. Papaioannou, Bayesian updating with structural reliability methods, J. Eng. Mech. 141 (3) (2015) 04014134.
[16] F.A. DiazDelaO, A. Garbuno-Inigo, S.K. Au, I. Yoshida, Bayesian updating and model class selection with subset simulation, Comput. Methods Appl. Mech. Engrg. 317 (2017) 1102–1121.
[17] W. Betz, I. Papaioannou, J.L. Beck, D. Straub, Bayesian inference with subset simulation: Strategies and improvements, Comput. Methods Appl. Mech. Engrg. 331 (2018) 72–93.
[18] P. Sengupta, S. Chakraborty, A two-stage Bayesian model updating framework based on an iterative model reduction technique using modal responses, Comput. Methods Appl. Mech. Engrg. 417 (Part A, 1) (2023) 116448.
[19] Jia-Hua Yang, Wen-Yue Liu, Yong-Hui An, Heung-Fai Lam, Enhanced adaptive sequential Monte Carlo method for Bayesian model class selection by quantifying data fit and information gain, Mech. Syst. Signal Process. 206 (2024) 110792.
[20] Silvia Monchetti, Cecilia Viscardi, Michele Betti, Francesco Clementi, Comparison between Bayesian updating and approximate Bayesian computation for model identification of masonry towers through dynamic data, Bull. Earthq. Eng. 22 (2024) 3491–3509.
[21] Suzana Ereiz, Ivan Duvnjak, Javier fernando jim'enez-alonso. Review of finite element model updating methods for structural applications, Structures 41 (2022) 684–723.
[22] Seung-Seop Jin, Young-Soo Park, SungTae Kim, Young-Hwan Park, Model updating based on mixed-integer nonlinear programming under model-form uncertainty in finite element model, Eng. Comput. 37 (2021) 3699–3725.
[23] J. Zeng, Y.H. Kim, Probabilistic damage detection and identification of coupled structural parameters using Bayesian model updating with added mass, J. Sound Vib. (2022) 117275.
[24] E.K. Henikish, A. Das, S. Bansal, On the Bayesian model updating based on model reduction using complex modal data for damage detection, J. Sound Vib. 556 (2023) 117712.
[25] Y. Yuan, F.T. Au, D. Yang, J. Zhang, Active learning structural model updating of a multisensory system based on kriging method and Bayesian inference, Computer-Aided Civ. Infrastruct. Eng. 38 (2023) 353–371.
[26] T. Yin, A practical bayesian framework for structural model updating and prediction, ASCE-ASME J. Risk Uncertain Eng. Syst. Part A Civ. Eng. 8 (2022) 1–15.
[27] R.P. Kiran, S. Bansal, Finite element model updating and damage detection using strain-based modal data in the Bayesian framework, J. Sound Vib. 584 (2024) 118457.
[28] J. Waeytens, B. Rosi'c, P.E. Charbonnel, E. Merliot, D. Siegert, X. Chapeleau, R. Vidal, V. le Corvec, L.M. Cottineau, Model updating techniques for damage detection in concrete beam using optical fiber strain measurement device, Eng. Struct. 129 (2016) 2–10.
[29] K. Csill'ery, M.G. Blum, O.E. Gaggiotti, O. François, Approximate Bayesian computation (ABC) in practice, Trends Ecol. Evol. 25 (2010) 410–418.
[30] M. Chiachio, J.L. Beck, J. Chiachio, G. Rus, Approximate Bayesian computation by subset simulation, SIAM J. Sci. Comput. 36 (2014) A1339–A1358.
[31] S.-K. Au, J.L. Beck, Estimation of small failure probabilities in high dimensions by subset simulation, Probabilistic Eng. Mech. 16 (2001) 263–277.
[32] M.K. Vakilzadeh, J.L. Beck, T. Abrahamsson, Using approximate bayesian computation by subset simulation for efficient posterior assessment of dynamic state-space model classes, SIAM J. Sci. Comput. 40 (1) (2018) B168–B195.
[33] J.-H. Yang, H.-F. Lam, An efficient adaptive sequential monte carlo method for bayesian model updating and damage detection, Struct. Control. Health Monit. 25 (12) (2018).
[34] J. Zeng, M.D. Todd, Z. Hu, Probabilistic damage detection using a new likelihood-free bayesian inference method, J. Civ. Struct. Health Monit. 13 (2) (2023) 319–341.
[35] P. Ni, Q. Han, X. Du, X. Cheng, Bayesian model updating of civil structures with likelihood-free inference approach and response reconstruction technique, Mech. Syst. Signal Process. 164 (2022) 108204.
[36] M.A. Fakih, M. Chiachío, S. Mustapha, A Bayesian approach for damage assessment in welded structures using lamb-wave surrogate models and minimal sensing, NDT & E Int. 128 (2022) 102626.
[37] A. Ben Abdessalem, N. Dervilis, D. Wagg, K. Worden, Model selection and parameter estimation in structural dynamics using approximate bayesian computation, Mech. Syst. Signal Process. 99 (2018) 306–325.
[38] T. Toni, D. Welch, N. Strelkowa, A. Ipsen, M.P.H. Stumpf, Approximate bayesian computation scheme for parameter inference and model selection in dynamical systems, J. R. Soc. 128 (2009) 187–202.
[39] T.G. Ritto, S. Beregi, D.A.W. Barton b, Reinforcement learning and approximate Bayesian computation (RL-ABC) for model selection and parameter calibration of time-varying systems, Mech. Syst. Signal Process. 200 (2023) 110458.
[40] T. Toni, D. Welch, N. Strelkowa, A. Ipsen, M.P.H. Stumpf, Approximate Bayesian computation scheme for parameter inference and model selection in dynamical systems, J. R. Soc. Interface 6 (2009) 187–202.
[41] C.P. Barnes, S. Filippi, M.P. Stumpf, T. Thorne, Considerate approaches to constructing summary statistics for ABC model selection, Stat. Comput. 22 (6) (2012) 1181–1197.
[42] R.G. Everitt, A.M. Johansen, E. Rowing, M. Evdemon-Hogan, Bayesian model comparison with un-normalised likelihoods, Stat. Comput. 27 (2) (2017) 403–422.
[43] V.M. Ong, D.J. Nott, M.N. Tran, S.A. Sisson, C.C. Drovandi, Variational Bayes with synthetic likelihood, Stat. Comput. 28 (4) (2018) 971–988.
[44] J.K. Pritchard, M.T. Seielstad, A. Perez-Lezaun, M.W. Feldman, Population growth of human y chromosomes: a study of y chromosome microsatellites, Mol. Biol. Evol. 16 (12) (1999) 1791–1798.
[45] M. Sunnaker, A.G. Busetto, E. Numminen, J. Corander, M. Foll, C. Dessimoz, Approximate Bayesian computation, PLOS Comput. Biol. 9 (1) (2013) e1002803.
[46] A. Ben Abdessalem, N. Dervilis, D. Wagg, K. Worden, Model selection and parameter estimation of dynamical systems using a novel variant of approximate Bayesian computation, Mech. Syst. Signal Process. 122 (2019) 364–386.
[47] M.A. Beaumont, W. Zhang, D.J. Balding, Approximate Bayesian computation in population genetics, Genetics 162 (4) (2002) 2025–2035.
[48] P.J. Rousseeuw, K.V, Driessen: A fast algorithm for the minimum covariance deteriminant estimator, Technometrics 41 (1999) 212–223.
[49] S.D. Bay, M. Schwabacher, Mining distance-based outliers in near linear time with randomization and a simple pruning rule, in: Proceedings of Ninth ACM SIGKDD International Conference on Knowledge Discovery and Data Mining, Washington, DC, USA, 2003, pp. 29–38.
[50] N. Moshtagh, Minimum Volume Enclosing Ellipsoid, Convex optimisation, 2005.
[51] L.G. Khachiyan, Rounding of polytopes in the real number model of computation, Math. Oper. Res. 21 (2) (1996) 307–320.
[52] N. Dervilis, E.J. Cross, R.J. Barthorpe, K. Worden, Robust methods of inclusive outlier analysis for structural health monitoring, J. Sound Vib. 333 (20) (2014) 5181–5195.
[53] N. Dervilis, K. Worden, E. Cross, On robust regression analysis as a means of exploring environmental and operational conditions for SHM data, J. Sound Vib. 347 (2015) 279–296.
[54] P. Kumar, E. Yildirim, Minimum-volume enclosing ellipsoids and core sets, J. Optim. Theory Appl. 126 (1) (2005) 1–21.
[55] P. Sun, R.M. Freund, Computation of minimum-volume covering ellipsoids, Oper. Res. (2004) 690–706.

[56] J.R. Shaw, M. Bidges, M.P. Hobson, Efficient Bayesian inference for multimodal problems in cosmology, Mon. Not. R. Astron. Soc. 000 (2006) 1–7.
[57] Feng Qian, Wei Zheng, An evolutionary nested sampling algorithm for Bayesian model updating and model selection using modal measurement. 140 12017, Pages 298-307.
[58] Israel Alejandro Hernández-González, Enrique Garcí.a-Macías, Towards a comprehensive damage identification of structures through populations of competing models, Eng. Comput. 40 (2024) 3157–3174.
[59] J.T. Kim, N. Stubbs, Model-uncertainty impact and damage detection accuracy in plate girder, J. Struct. Eng. 121 (10) (1995) 1409–1417.
[60] A. Esfandiari, F. Bakhtiari-Nejad, A. Rahai, M. Sanayei, Structural model updating using frequency response function and quasi-linear sensitivity equation, J. Sound Vib. 326 (2009) 557–573.
[61] N. Chopin, A sequential particle filter method for static models, Biometrica 89 (3) (2002) 539–552.
[62] L. Liu, H. Chen, S. Wang, J. Zeng, A comparative study of single-chain and multi-chain MCMC algorithms for Bayesian model updating-based structural damage detection, Appl. Sci. 14 (2024) 8514.
[63] C. Ziegler, R.J. Dyson, I.G. Johnston, Model selection and parameter estimation for root architecture models using likelihood-free inference, J R Soc Interface. 16 (156) (2019) 20190293.
[64] M. Rabhi, A.B. Abdessalem, L. Saintis, B. Castanier, R. Sohoin, Discrimination between accelerated life models via approximate Bayesian computation, Qual. Rel. Eng. Int. 39 (3) (2023) 1058–1082.